RNA EXPRESSION PATTERNS IN PANCREATIC INTRAEPITHELIAL NEOPLASIA

By

Michael Ayars

A dissertation submitted to the Johns Hopkins University in conformity with the requirement for the degree of Doctor of Philosophy

Baltimore, Maryland

ABSTRACT

Pancreatic ductal adenocarcinoma (PDAC) is a genetic disease that evolves from precursor lesions, the most common of which are pancreatic intraepithelial neoplasia (PanINs). In this study, we present RNA-sequencing analysis of PanINs. We identify genes subject to differential expression between PanIN and normal pancreatic duct and between low-grade and high-grade PanIN. One novel gene identified as overexpressed in PanIN and invasive pancreatic ductal adenocarcinoma is interleukin-2 receptor subunit gamma (IL2RG) which encodes the common gamma chain. CRISPR-mediated depletion of IL2RG in orthotopically implanted pancreatic cancer cells resulted in attenuated tumor growth in mice. Additionally, we examine the therapeutic sensitivities of inactivation of Ataxia Telangiectasia Mutated (ATM), a critical DNA repair gene not infrequently mutated in pancreatic cancers. We find that ATM-depleted pancreatic cancer cell lines have no added sensitivity to several chemotherapeutic agents, but are markedly sensitive to radiotherapy. These data contribute new considerations for existing therapeutic candidates and open the door to a new set of potentially-targetable pathways for disease management.

Advisor: Dr. Michael Goggins, M.D.

Readers: Drs. Michael Goggins, M.D. and James Eshleman, M.D., Ph.D.

ACKNOWLEDGEMENTS

TABLE OF CONTENTS

LIST OF TABLES

LIST OF FIGURES

Chapter 1. Introduction

Pancreatic cancer: the present overview

Pancreatic cancer is the third-leading cause of cancer death in the USA, with a 5-year survival rate of 8%[1]. Surgical resection remains the best treatment option for pancreatic cancer[2, 3], however, less than 20% of patients are diagnosed with resectable cancers. Although PanINs, the most common precursor lesion, are thought to exist in a treatable, pre-symptomatic state for years or decades prior to becoming invasive, no non-invasive screening test exists to detect them. Instead, cancers are almost universally diagnosed at an intavasive stage unamenable to therapy. Surgery is the only curative treatment option for pancreatic cancer, but it is not possible in most cases. However, pancreatic resection with curative intent does not remove the cancer completely in many cases due to microscopically positive margins[4] and/or the presence of micrometastases[5], underlining a need for adjuvant therapy. Recurrence of pancreatic cancer is common, and 5-year survival after pancreatic resection is only ~ 20%[6]. Systemic chemotherapy can be used to downstage advanced cancers or reduce the chance of post-operative recurrence[7], but current options confer limited benefit and have high toxicities[8]. Many novel therapies have been evaluated for pancreatic cancer and most of these have failed to show benefit. The role of adjuvant vs. neoadjuvant therapy and the role of radiotherapy is still not clear and requires further study[9-11]. Thus, the high mortality rate of pancreatic cancer is largely owed to two factors: an inability to detect early, low-stage cancer and pre-invasive lesions, and a paucity of effective cancer therapy. Examination of the molecular aberrations characterizing PanINs and PDAC has the potential to reveal targets for early detection and treatment and to better understand the biology of the disease. In chapter 2, we present the results of RNA sequencing analysis from PanIN samples and identify IL2RG as a novel overexpressed gene in pancreatic cancer. In chapter 3 we describe the use of bioinformatics tools to identify novel transcripts in PanINs. In chapter 4, we examine the impact of loss of the DNA repair protein Ataxia Telangiectasia

Mutated that occurs in a subset of cancers and show evidence for their exquisite sensitivity to fractionated radiotherapy.

Genetic alterations in Pancreatic ductal adenocarcinoma

The most common form of pancreatic cancer is pancreatic ductal adenocarcinoma (PDAC), which accounts for >85% of cases [12]. The acquired genetic abnormalities of PDAC are extensive and well-understood. The four most commonly mutated genes are *KRAS*[13], *CDKN2A*[14], *TP53*[15], and *SMAD4/DPC4*[16]. Comprehensive genetic analysis of PDAC found tumors to contain genetic alterations falling into core signaling pathways that were individually altered in 67 to 100% of cases[17]. Many of these pathways are unsurprising: perturbation of *KRAS* signaling, Wnt signaling, and Hedgehog signaling promote proliferation, while disruption of DNA damage control, chromatin regulation, and apoptosis pathways support an accumulation of mutations and resistance to cell death from their detection. Others relate to additional growth signaling, disruption of the native microenvironment, and invasion. In all, these core pathways illustrate a roadmap of the changes necessary for PDAC to achieve expansion, invasion, and metastasis as well as potential targets for screening and therapy.

Precursors to PDAC

PDAC is understood to arise from the stepwise progression of one of three precursor lesions: pancreatic intraepithelial neoplasia (PanINs), intraductal papillary neoplasms (IPMNs), and mucinous cystic neoplasms (MCNs) [18]. PanINs are thought to be the precursors to an overwhelming majority of PDAC and are distinct from the other two precursors in being microscopic (<5 mm) and currently undetectable by non-invasive tests. While PanINs are

thought be to be common in adults, few of these lesions ever progress to PanIN-3 (carcinoma *in situ)*, with one estimate from Terhune *et al* suggesting the proportion to be as low as 1%.[19] Between the complications that can arise from pancreatic surgery, the lack of a non-invasive screen for PanINs, and the low risk of progression of PanIN-1, much energy has been put into identifying risk factors for developing PanIN and to understand the molecular progression of PanIN.

Known risk factors for pancreatic cancer include a host of inherited germline mutations in *BRCA2*[20]*, p16*[21]*, ATM*[22]*, STK11*[23]*, PRSS1*[24]*, and PALB2*[25]. Chronic pancreatitis is a key risk factor for pancreatic cancer[26]. Germline mutations in *PRSS1* predispose patients to developing recurrent acute pancreatitis at a young age so that carriers have a lifetime risk of pancreatic cancer of ~30%. Heterozygous carriers of mutations in the pancreatitis risk genes, *CFTR* and *SPINK1*[24],, are at increased risk of developing chronic pancreatitis but these are considered modifier genes as most carriers will not develop pancreatitis or pancreatic cancer [27]. In mouse models, cerulein-induced pancreatitis accelerates the development of PanINs [28, 29]. The PanScan Project, a multi-stage genome wide association study undertaken by the Pancreatic Cancer Cohort Consortium, has identified single nucleotide polymorphisms associated with increased risk of pancreatic cancer in multiple loci including *ABO*, *TERT*, *PDX-1* [30]and nuclear receptor subfamily 5[31]. Environmental and lifestyle factors also play a role in pancreatic cancer development. Comprehensive meta-analyses have established an elevated relative risk for pancreatic cancer associated with obesity[32] [33]. Many studies have also linked diabetes mellitus[34-37] and smoking[37-39] to pancreatic cancer. Smoking has been found to double the average risk of developing pancreatic cancer, and pancreatic cancers in smokers have a higher mutational burden than those in nonsmokers[40]. These factors, in isolation or combination, contribute to the risk of developing PDAC.

PanIN[41] Progression Model

In a progression model established by Hruban *et al*[42], 3 grades of PanINs can be distinguished histologically. PanIN-1s have a flat or micropapillary architecture, with tall columnar cells and an accumulation of intracellular mucin. PanIN-2s are papillary and display mild cytological atypia: nuclear crowding, depolarization, and hyperchromasia. PanIN-3s display a dramatic breakdown of ductal architecture, with luminal necrosis and budding of cells into the lumen. They also possess more extreme cytologic atypia with dystrophic goblet cells, prominent nucleoli, and mitotic figures[43]. These histological changes correlate with increasing accumulations of the common mutations found in PDAC. Telomere shortening is near universal in both PDAC and PanINs, and is commonly the first observable event in PanIN-1s[44]. Another early event is activating mutations in the K-ras gene[45] which are found in ~90% of PanIN-1 lesions matching the >90% of PDAC[13, 19]. Loss of p16 expression occurs in 30% of PanIN1s, 55% of PanIN2s, 70% of PanIN3s, and 95% of PDAC, suggesting a role for p16 in progression rather than initiation[45, 46]. Loss of *p16* generally occurs due to mutation or copy number loss, but can also be the result of promoter hypermethylation[47]. PanIN lesions in the context of chronic pancreatitis are especially prone to p16 loss, marking this change as one way that inflammation may contribute to progression[48]. Later genetic events in PanINs include inactivating mutation of TP53 (30-50%)[49] and homozygous deletion of DPC4/SMAD4 (30%)[41, 46], generally being observed only in PanIN-3 and PDAC.

Epigenetic alterations have also been identified in PanIN but are relatively understudied compared to the literature examining epigenetic alterations in PDAC. Of a list of eight genes hypermethylated in invasive pancreatic cancer, Sato *et al* showed that at least one of the eight was aberrantly hypermethylated in 68% of 65 tested PanIN lesions[50]. Additionally, PanIN3s were aberrantly methylated at an average of 2.9 loci in comparison to 1.1 loci in PanIN1s and PanIN2s (P=0.01), suggesting CpG hypermethylation progressively increases with progression.

Although many molecular alterations have been identified in PanINs, but perhaps surprisingly, it is still not known what molecular events are required for a PanIN-3 lesion to progress to an invasive PDAC. Histologically, PanIN3s are rarely found in the absence of PDAC, and can be difficult to distinguish from PDAC due in part to the latter's propensity for cancerization of nearby ducts [43, 46]. PDAC also frequently overgrows PanIN-3. Both PDAC and PanINs harbor a high mutational burden of what are thought to be largely passenger mutations, making identification of novel drivers difficult[51]. The size and low cellularity of these lesions constrain many researchers to using bulk tissue to characterize these lesions, adding a high potential for normal contamination and making isolation of PanIN3 signal from cancer even more difficult. In a step to clarify this, Murphy *et al* utilized exome sequencing of microdissected samples from PDAC and adjacent PanINs. They determined that >50% similarity existed between the mutations of 10 of the 15 isolated PanINs and their associated invasive cancer which suggested that the PanIN lesions were often different clones to the PDAC[51].

Chapter 2. Expression of IL2RG in PanINs

Major transcriptional changes occur during PDAC development. Jones *et al* found that gene sets in the same 12 core signaling pathways commonly subject to mutation in PDAC were also enriched in differentially expressed genes compared to gene sets outside of these pathways ($P < 0.001$)[17]. The number of differentially expressed genes in PDAC samples is extensive and has been reviewed elsewhere [52]. Some of the well-known differentially expressed genes in PDAC include mesothelin [53, 54] which has for many years been studied as an immunotherapy target[55]. Other transcriptionally upregulated targets that have been evaluated as potential biomarkers for diagnosis include osteopontin[56], MIC-1[57], several mucins[58], and microRNAs (miRNAs) including miR200[59] and miR1290[60]. Numerous genes have also been silenced in PDACs many of them epigenetically, including *TFPI-2*[61], *RELN*[62], *EYA2*[63], *SIP-1*[64] and many others.

Fewer studies have been performed to determine the transcriptional changes in PanINs. Expression analysis using cDNA microarrays by Prasad *et al* identified 49 differentially expressed genes in early PanIN lesions including extra-pancreatic foregut markers pepsinogen C, *MUC6, KLF4, and TFF1* transcripts[65]. Another microarray study established *HOXB2* as overexpressed in 38% of PDAC samples and 15% of PanIN samples[66]. miRNAs overexpressed in PDAC including miR-21, miR-155, and miR-221 have also been shown to be overexpressed in high-grade PanINs[67]. Sequencing of PanIN RNA is constrained by the difficulty of obtaining RNA from PanINs. The microscopic scale of the lesions and their heterogeneous makeup necessitates the use of laser microdissection. The extremely high level of RNase activity in pancreas compared to other tissues[68] also makes it difficult to retrieve RNA of a yield and quality permissive to RNA-sequencing.

Analyzing RNA-seq data

As interest in RNA sequencing has grown in recent years, the number of available tools and strategies for analysis have increased in tandem. In this study, we first use RSEM (RNA-Seq

by Expectation Maximization) (http://deweylab.github.io/RSEM/) to quantify the transcript and gene abundances from paired-end reads in our samples. A major advantage of RSEM is its ability to compensate for the ambiguity arising from reads that map to multiple transcripts/genes, a frequent and biologically-legitimate result in eukaryotic genomes. RSEM does this by assigning reads to their most likely of many possible mapping loci based on a statistical model the tool generates from read quality and fragment length distribution[69]. On simulated data, RSEM has proven especially robust in comparison to other tools when using paired-end reads at estimating the relative abundance of individual isoforms within a gene[70].

Limma is a program used to calculate differential expression from our RSEM counts (https://bioconductor.org/packages/release/bioc/html/limma.html). Our reason for choosing limma is that it is superior to other approaches at handling small sample sizes, due to its use of a parametric, empirical Bayes method. In accounting for residual variance of genes, strength from other genes can be 'borrowed' due to the fact that all of them are fitted with the same linear model[71, 72]. As our normal duct sample group has only three samples, this is an effective approach to stabilizing inference for our differential expression comparison.

Neotranscription

In the pursuit of identifying biomarkers for cancer screening, much focus has been placed on identifying overexpression of normal proteins. Serum levels of Prostate Specific Antigen (PSA) has seen use as a screening tool and prognostic marker for prostate cancer[73], but typically such markers are not very specific for cancer because overexpression can occur from non-neoplastic causes [74]. Mesothelin is detectable in serum and consistently overexpressed by pancreatic cancer, but is not a useful diagnostic marker because it is also expressed in normal mesothelial linings[75].

One strategy to circumvent these problems is to focus on 'neotranscription', cancer's propensity to generate novel coding transcripts. One mechanism that achieves this is alternative transcription, in which the normal splicing machinery of the cell aberrantly splices coding transcripts to exclude and include a combination of novel exons. A more stable mechanism is gene fusions, where chromosome breakage and rearrangement results in coding sequences from two different genes being fused into one novel transcript. This can result in a potential oncogene being fused to the promoter of a highly expressed gene or, in rare cases, a hybrid protein with totally novel (and oncogenic) functionality. The most famous of these events is the BCR/ABL fusion, a driving event of chronic myeloid leukemia[76] that has proven to be one of the greatest successes of targeted therapy [77].

Several challenges have made the detection of novel neotranscription difficult to identify. Alternative splicing is commonplace, occurring in most multi-exon genes in normal cells[78]. As with the differential expression manifest in cancer cells, the vast majority of these events are likely to be passengers rather than drivers, and functional consequences of the inclusion or exclusion of different exons are rarely obvious by sequence alone. Fusion events are much less common and are usually functionally significant. Their identification requires the alignment of paired reads flanking the breakpoint (or a single read spanning it) to two different genomic loci, which is difficult for existing tools to distinguish from sequencing artifacts.

Limited neotranscription data exists for pancreatic cancer. A characterization of the PDAC splicesome by microarray and RT-PCR found that the range of diversity seen in alternative splicing actually pointedly decreased in pancreatic cancer cell lines in comparison to normal cell lines. Additionally, the expression of a number of splicing factors was decreased in high grade pancreatic cancers, in contrast to other cancers[79]. In a study of 100 pancreatic cancers, 1,236 chromosomal rearrangement events led to the joining of two gene loci, 183 of which

involved an orientation and frame likely to produce a functional transcript[80]. An analysis using RNA-seq detected 50 productive fusion events in 13 PDAC samples[81].

Cytokine signaling Pathways in PDAC

Chronic and acute inflammation contribute a rich milieu of cytokines to the microenvironment that can be exploited by cancers to promote growth. Many of these cytokines work through the various JAK/STAT signaling pathways, in which the cytosolic transcription factor signal transducer and activator proteins (STATs) are phosphorylated by activated Janus kinases (JAKs)[82, 83]. One example is the inflammatory cytokine interleukin-6 (IL-6), which in genetically engineered mouse models of PDAC is needed for the maintenance and progression of PanINs[84] through the IL-6R/JAK1/STAT3 signaling axis. In PDAC, STAT3 blockade inhibits growth[85, 86].

IL-6 is just one of several inflammatory cytokines that mediates JAK/STAT signaling. Our transcriptional profiling of PanINs led to the identification of IL2RG as an overexpressed cytokine receptor. IL2RG binds to Interleukins 2, 4, 7, 9, 15, and 21 and once the IL2 receptor complex binds to ligand, IL2RG activates JAK1[87], JAK3[87], and phosphatidylinositol-3 (PI-3) kinase[88]. This role makes IL2RG critical to the maintenance and functionality of the immune system; its loss causes severe combined immunodeficiency syndrome (SCID), a near-total absence of T and B-cells[89]. IL2RG cytokine ligands have varied, overlapping downstream effects on proliferation, differentiation, and survival that have led to them being frequently co-opted in haematopoietic malignancies[90-92]. IL-4 and IL-4R are upregulated in and induce proliferation in a variety of solid cancers, including colon[93], thyroid[94] and prostate[95].

MATERIALS AND METHODS

<u>Laser microdissection</u>

Gross tissue samples were mounted on activated polyethylene naphthalate (PEN) slides and histologically graded for 3 normal ducts, 4 PanIN1A/Bs, 5 PanIN2s, and 9 PanIN3s. Slides were immersed in RNAlater (ThermoFisher Scientific) and stored at -80º C. Slides were stained with Cresyl Violet and laser microdissected on a Leica LMD6 within 20 minutes of thawing. RNA was harvested from microdissected cells (Arcturus PicoPure RNA Isolation Kit) and examined for concentration and quality using an Agilent Bioanalyzer with RNA 6000 Pico reagents. Only samples with an RNA integrity score (RIN) score of >7 were sequenced.

<u>RNA-sequencing</u>

13 of the harvested samples (1 normal duct, 2 PanIN1s, 3 PanIN2s, and 7 PanIN3s) were converted to cDNA libraries using a Nugen Ovation RNA-Seq V2 kit with the SOLiD fragment protocol and sequenced on an Applied Biosystems SOLiD v. 5500 Wildfire. Reads from this set were aligned using the Bioscope v1.3 Whole Transcriptome Plugin. FPKM values were calculated using HTSeq-count (http://www-huber.embl.de/HTSeq/doc/overview.html). The remaining 8 samples (2 normal duct, 2 PanIN1s, 2 PanIN2s, and 2 PanIN3s) were converted to cDNA libraries using the Nugen kit with the TruSeq protocol and sequenced on an Illumina HiSeq 2500. Alignments and FPKM values for these samples were generated using rsem-1.2.9 (http://deweylab.github.io/RSEM/). FPKM values from the two sets of samples were combined using ComBat for batch removal. Lists of differentially-expressed genes in comparisons between the different grades of PanINs and normal epithelium were generated using limma with an empirical Bayes method and fitted intensity trend. Pathway analysis was conducted using the Pathview Bioconductor package and KEGG database.

Immunohistochemistry:

The HRP EnVision[+] System (DAKO Corp.) was used to evaluate IL2RG protein expression in tissue microarrays (TMAs) using a rabbit anti-IL2RG antibody (Sigma-Aldrich; 1:250 dilution) using methods previously described[96]. Infiltrating lymphocytes were used as a positive control. The relative intensity of labeling in neoplastic and normal duct cells was qualitatively assessed as 'negative', 'weak', 'intermediate', or 'strong' for each TMA core based on the percentage of cells labeling.

Cell culture:

Mouse pancreatic cancer cell lines TB31456 and TB32043 were generously provided by Dr. Tuveson (Cold Spring Harbor Laboratory). The mouse pancreatic cancer cell line bkpc58 was generated by Dr. Anne MacGregor in the laboratory of Christine Iacobuzio-Donahue. All human and mouse cell lines were cultured in DMEM supplemented with 10% heat-inactivated fetal bovine serum, 100 units/ml penicillin, 100 µg/ml streptomycin (Gibco), and 2.5 mg/500 ml plasmocin (Invivogen) in 95% air and 5% carbon dioxide at 37º C.

Organoid culture:

10,000 cells were pelleted at 4º C and resuspended in 4º C matrigel. 50 ul of matrigel were pipetted into the center of wells on a 24-well plate and placed in a 37º C incubator for 15 minutes to solidify. 500 ul DMEM + 10% FBS + 1% penicillin/streptomycin was added to each well. Media was changed every 3-4 days and cells were observed for signs of spherical growth. Cells were passaged by aspirating media, adding ice-cold media to dissolve matrigel, and pipetting the well contents into a 15-ml tube. Organoids were pelleted, washed once with PBS, and resuspended in 4º C matrigel at a 1:2 dilution to seed additional wells.

Western blotting:

Total protein lysates were extracted in RIPA buffer (Roche Diagnostics, Indianapolis, IN) with cOmplete Mini tablets (Roche Diagnostics) and homogenized with a Bioruptor (Diagenode, Denville, NJ) for 8 cycles (30s high, 30S off).   Protein concentrations were determined using the Pierce BCA Protein Assay Kit (ThermoScientific, Waltham, MA). Membranes were incubated overnight at 4º C with primary antibodies: rabbit anti-IL2RG (Santa Cruz Biotechnology, Dallas, TX), rabbit anti-JAK3 (Cell Signaling Technology, Danvers, MA), or goat anti-Actin (Santa Cruz Biotechnology). Membranes were incubated with horseradish peroxidase (HRP)-conjugated secondary antibody in 5% dry milk for 1 hour. Bound antibody was detected with a Pierce ECL Plus kit (ThermoScientific).

Generation of CRISPR plasmids

CRISPR knockout experiments were performed with Cas9 nickase (Cas9n) enzymes guided by paired sgRNA sequences to mitigate off-target effects as previously described[97]. Paired sgRNA sequences targeting IL2RG on the X-chromosome were designed using the MIT CRISPR Design Tool (crispr.mit.edu) and synthesized by Integrated DNA Technologies: Pair 1: 5'-TCTTAGTCCTTCAGCTGCTC-3', 5'-GAGGGCAGGGTGGAGCTCCA-3'. Pair 2: 5'-TCCAGAGGTTCAGTGCTTTG-3', 5'-TAGAGTACATGAATTGCACT-3'. SgRNA oligonucleotides were annealed and ligated into digested pSpCas9n(BB)-2A-GFP (PX461) (Addgene, Cambridge, MA) utilizing the following reaction mix: 1 µl px461 (100 ng), 1 µl annealed oligonucleotides (0.5 µM), 1 µl Bbs1 Fast-Digest (ThermoFisher Scientific), 2 10x Fast-Digest buffer (ThermoFisher Scientific), 1 µl T4 Ligase (ThermoFisher Scientific), 14 µl ddH20. This mix was incubated in a 37ºC water bath for 2 hours and then transformed into Stbl3 expression bacteria by heat shock (ThermoFisher Scientific). Bacteria were selected by antibiotic resistance on Ampicillin plates (100 µg/ml) and harvested for plasmid using a QIAprep Plasmid

Miniprep kit (Qiagen, Germantown, MD). Harvested plasmid was Sanger sequenced to confirm appropriate insertion.

Generation of CRISPR knockout clones:

Cells were plated on 24-well plates at $1.3x10^5$ cells/well 16-24 hours before transfection. Each well was transfected with 250 ng of each paired Cas9n plasmid (500 ng total) using Lipofectamine 2000 (ThermoScientific Fisher) according to the manufacturer's protocol. The TB32043 cell line was transfected with the IL2RG-targeting pair 1 Cas9n plasmids and the bkpc58 cell line was transfected with the IL2RG-targeting pair 2 Cas9n plasmids. 3 days after transfection, cells were flow sorted for GFP expression using a BSL 2 FACSAria II instrument into 96 well plates at 1 cell per well. These cells were grown for 3 weeks before harvesting for DNA to test for the presence of CRISPR deletions. Genomic DNA from the female TB32043 cell line was cloned into TOPO vectors for Sanger sequencing according to the manufacturer's protocol (TOPO TA Cloning Kit for Sequencing, ThermoScientific Fisher).

Xenograft dissections:

$3x10^5$ TB32043 cells or $1x10^5$ bkpc58 cells were injected into the pancreas of 6-10 week old C57BL/6J mice (The Jackson Laboratory, Bar Harbor, ME). Mice were sutured and followed daily for survival. After 21 or 23 days, mice injected with TB32043 cells or bkpc58 cells respectively were sacrificed and dissected. Cancers were weighed, immersed in RIPA buffer, and homogenized with a Tissue Disruptor to isolate protein for western blotting.

In vitro proliferation:

Pancreatic cancer cell lines were seeded in the center 60 wells of 96-well plates at 3,000 cells/well. After 24 hours, media was replaced with normal media, L929-conditioned media, or normal media supplemented with 100 ng/ul an IL2RG ligand: IL4, GM-CSF, or IL7. After 72

hours of treatment, AlamarBlue was added to each well and cells were incubated for an additional 4 hours. Absorbance was measured at 490 nm using a BMG FluoStar Galaxy instrument.

<u>Statistical Analysis</u>

Descriptive statistical values and plots were generated using the Microsoft Excel software packages, Graphpad Prism 6.0, and R bioconductor. For RNA sequencing analysis, lists of differentially expressed genes were generated using limma with an empirical Bayes method and fitted intensity trend. Presented lists of genes were filtered to those differentially expressed with a q-value of < 0.1.

RESULTS

Differential expression in PanIN3s

21 tissue samples were laser microdissected and processed for RNA-sequencing analysis: 3 normal pancreatic ducts, 4 PanIN-1, 5 PanIN-2, and 7 PanIN-3 samples. In our principle component analysis of mRNA expression, we found that with one outlying exception, PanIN-3 samples were the most divergent among PanINs from the normal ducts (Figure 2). Using a q-value threshold of 0.1, we identified 1723 genes differentially expressed between normal duct samples and PanIN-3 samples. Table 1 lists the most differentially expressed genes with reported functional roles in cancer.

Some of the genes identified as overexpressed in PanIN-3 samples have been reported to have oncogenic properties. REG4 overexpression enhances the viability of PDAC cells. REG4 protein can be detected in the sera of patients with PDAC, although REG4 is expressed in other

normal tissues and has not been shown to be a specific circulating marker of PDAC [98]. FXYD3, which encodes FXYD Domain Containing Ion Transport Regulator 3, is similarly overexpressed in both PDAC and PanINs and has been reported to influence pancreatic cancer growth[99]. WFDC2 (HE4), a well known circulating marker of ovarian cancer, has been shown to be overexpressed in pancreatic cancers and elevated HE4 levels have been described in the sera of some patients with PDAC[100].

Concurrently, several genes with cancer suppressive properties known to be silenced in PDAC were also found to be markedly underexpressed in the PanIN3 samples. TFPI2 and RELN are both frequent targets of silencing by DNA hypermethylation in pancreatic cancer and IPMNs[62, 101],[102]. Loss of expression of p21, which was also found to be underexpressed in our PanIN3 samples, has also been reported to occur in pancreatic cancer and to be associated with metastasis, dedifferentiation, and poor prognosis[103].

We generated lists of differentially expressed genes between each PanIN grade and normal duct samples. All lists included here are of the 50 genes with the lowest adjusted p-value for differential expression within their comparison. In Table 2, we list the genes exclusively overexpressed in PanIN3 samples in comparison to normal duct samples (i.e. not overexpressed in PanIN1 or PanIN2 samples). In Table 3, we list the genes overexpressed in a pooled sample group of all 3 PanIN grades in comparison to normal duct samples. Finally in table 4, we list the genes underexpressed in PanIN3 samples in comparison to normal duct samples.

We used immunohistochemistry to examine the expression of the protein products of several genes identified as differentially expressed by RNA-seq. Through immunohistochemistry analysis of TMAs, we found REG4 to be overexpressed at the protein level in PDAC and PanINs. The overwhelming majority of cores containing normal pancreatic duct featured weak immunolabeling of REG4 (87.5%, 14/16) and the remaining two were intermediately labeled. In

the PanIN-1A cores, 40% (2/5) were weakly labeled, 20% (1/5) were intermediately labeled, and 40% (2/5) were strongly labeled. Of the PanIN-1B cores, 11.11% (1/9) cores were intermediately labeled, and 88.89% (8/9) cores were strongly labeled. Of the PanIN-2 cores, 42.85% (3/7) cores were intermediately labeled and 57.14% (4/7) cores were strongly labeled. Of the PanIN-3 cores, 20% (2/10) cores were intermediately labeled and 80% (8/10) were strongly labeled. Of the PDAC cores, 100% (5/5) were strongly labeled. (Figure 1).

IL2RG expression

While many of the differentially expressed genes found in PanIN have been reported to be similarly differentially expressed in PDAC, there were notable exceptions such as *IL2RG*. In our dataset, *IL2RG* is overexpressed in PanIN3 samples by an average log fold change of 4.43 over normal ducts (Figure 1A).

To confirm that our microdissection was performed to isolate pure cell populations, we checked if other lymphocyte markers were enriched in our PanIN samples. PTPRC (CD45) and CD3D are two transcriptional markers for lymphocytes. We find no significant correlation between lymphocyte signature genes and IL2RG expression in our samples (PTPRC =-0.2454545, p-value = 0.2822, CD3D = -0.2285714, p-value = 0.3175), suggesting that IL2RG overexpression is not the result of increasing lymphocyte infiltration in higher grade PanINs that was not microdissected (Figure 1B). Overlaying our expression data on the Kyoto Encyclopedia of Genes and Genomes (KEGG) pathway for JAK-STAT signaling, we observe that several other genes downstream of IL2RG signaling are up- or downregulated in a direction consistent with pathway activation (Figure 5).

We sought to assess protein expression of Il2rg in patient PDAC, PanIN, and IPMN lesions by immunohistochemistry on tissue microarray slides (Figure 2). The PanIN TMA recapitulated our sequencing results: normal ducts stained only weakly or negatively while

PanINs showed a progressively increase in the percentage of intermediate and strong staining lesions with grade (1A: 0/7 cases, 0%, 1B: 1/5 cases, 20%, 2: 4/12 cases, 33%, 3: 6/14 cases, 43%, cancer: 5/9 cases, 56%). IPMNs also displayed overexpression compared to normal pancreatic ducts. Similarly, in the PDAC TMAs, the majority of cancer samples presented with intermediate or strong labeling (38/53 cases, 71.70%) while the vast majority of normal ducts featured negative or weak staining (27/29 cases, 93.10%).

The factors regulating expression of *IL2RG* remain unknown. Although a direct link has not yet been demonstrated, the *MECOM* transcription factor (MDS1 and EVI1 complex locus) has a consensus sequence binding site in the *IL2RG* promoter identified through the Transfac database (http://www.gene-regulation.com/pub/databases.html). MECOM has also been found to induce KRAS through suppression of the KRAS-inhibitory microRNA-96 in pancreatic cancer[104]. In our dataset, MECOM RNA is overexpressed in PanIN3 samples by a log fold change of 3.77 over normal ducts (Table 1).

We next examined Il2rg protein expression in human PDAC cell lines. By western blotting, we were unable to detect Il2rg in any of our tested cell lines (Figure 7) consistent with the lack of RNA expression in pancreatic cancer cell lines by Serial Analysis of Gene Expression (SAGE); elevated levels of *IL2RG* transcripts were present in primary PDAC but no expression was present in human PDAC cell lines[17]. There is evidence that Il2rg expression is rapidly lost *in vitro* [105]. This is consistent with the known rapid change in expression of Il2rg and its downstream binding partner Jak3 and subsequent pathway activation/inactivation in response to stimuli in lymphocytes[106].

With this in mind, we hypothesized that *IL2RG* expression may be dependent on *in vivo* signaling and restored in that context. We performed immunohistochemistry analysis on

orthotopically implanted mouse PDAC cell line and identified two of five with expression of Il2rg (Figure 4A).

These cell lines were cultured are harvested for protein to assay for Il2rg expression. In the absence of a suitable antibody for mouse Il2rg , but it is known that the expression of IL2RG and JAK3 are tightly linked [107]. We were unable to detect Jak3 in either cell line by western blot (Figure 4B), supporting the hypothesis that pancreatic cancers can express Il2rg *in vivo* but not *in vitro*. L929 is a fibroblast mouse cell line used to condition media for macrophage differentiation that secretes several cytokines including GM-CSF which has been reported to be an Il2rg ligand[108]. We found that conditioning our cell lines with L929-conditioned media did not induce *IL2RG* expression (data not shown).

We also examined if IL2RG expression could induced by growing pancreatic cancer cells as organoids but did not find pancreatic cancer organoids expressed Il2rg

Generation of IL2RG knockout clones using CRISPR/Cas9

We resolved to knockout *IL2RG* from mouse pancreatic cancer cell lines using the CRISPR/Cas9 system. Mouse cancer cells were chosen so that we could examine the effect of in vivo growth after IL2RG knockout. Cells were transfected with plasmids containing the Cas9 nickase enzyme and pairs of guide RNAs targeting exons 1, 2, and 3 of *IL2RG*. Clones were isolated and tested for genome editing by Sanger sequencing. We initially identified no clones featuring homozygous deletion of *IL2RG* but several heterozygotes. One of these heterozygotes was retransfected with the same *IL2RG*-targeting pair 1 plasmids and flow sorted as previously described. One of the resulting clones was Sanger sequenced and found to harbor a homozygous deletion in *IL2RG*. A second cell line was replaced with a male bkpc line to reduce the number of

alleles requiring editing as *IL2RG* is on the X-chromosome. Genomic DNA from a male bkpc58 clone was confirmed by Sanger sequencing to have a homozygous deletion in IL2RG.

The two clones identified with genomic deletions in *IL2RG* were a 32043 clone with a 52 base pair deletion in exon 1, and a bkpc58 clone with a 104 base pair deletion in exon 3 (Figure 4C).

Impact of IL2RG loss on the *in vitro* growth of cell lines

We hypothesized that it may be possible to induce IL2RG expression and response to IL2RG ligands in our cell lines. We treated our wild type and IL2RG knockout cell lines with L929 media to test this possibility. After three days of treatment, we assayed the number of metabolically-active cells using AlamarBlue (Figure 10). Although we observed a significant induction of proliferation in the wild type cells and not the IL2RG knockout cells in some experiments, this result proved inconsistent across replicates. We hypothesize that this may be the result of batch variance in the cytokine complement of our L929 media harvested on different dates.

We additionally tested whether proliferation could be induced by treatment with a high dose of Il2RG ligands. IL-4, GM-CSF, and IL-7 were selected based on the expression of downstream signaling targets observed in the PanINs highly-expressing IL2RG. We repeated our proliferation experiment replacing L929 media with normal media supplemented with 100 ng/ul of IL-4, GM-CSF, or IL-7 (Figure 11). In all three cases, we observed no significant induction of proliferation in wild type or IL2RG knockout cell lines.

Impact of IL2RG loss on the growth of orthotopically implanted pancreatic cancer cells

We compared the growth of the parental and knockout clones in vitro and found no significant difference (data not shown). We next injected our CRISPR *IL2RG* knockout cells into

mice to determine what effect *IL2RG* loss would have on *in vivo* tumorigenesis. After 21 days for

line 32043and 23 days for line bkpc58, injected mice were sacrificed and cancer weights were

compared. There was no significant difference in cancer growth between wild type and unedited

xenografts but a significant reduction in the weight of *IL2RG* knockout xenografts: TB32043

30.75% ± 10.43% (p-value = 0.0001), bkpc58 29.58% ± 12.58% (p-value = 0.0133)(Figure 5A).

Additionally, western blot analysis of the 32043 cell line xenografts showed significantly higher

expression of *JAK3* in the parental vs. knockout cells (p-value = 0.0156) (Figure 5B) consistent

with reduced pathway activation in the knockout cells.

DISCUSSION

In this study, we demonstrate that PanINs and PDAC overexpress the common gamma

chain, IL2RG. Our ability to detect this overexpression highlights the utility of using

microdissected samples for transcriptional profiling. CRISPR-induced truncating mutations of

IL2RG in two different cell lines resulted in significantly reduced cancer growth in orthotopic

xenografts and reduced expression of its signaling partner JAK3, supporting a functional role for

IL2RG in pancreatic cancer cells.

The lack of an in vitro model of IL2RG expression in pancreatic cancer cells presents

challenges for the further characterization of this pathway. In the literature, it has been reported

that a functional receptor hybridizing granulocyte/macrophage colony stimulating factor receptor

β (GM-CSFRβ) and IL2RG expression has been reported to be present in hematopoietic CD34^{+}

cells responding to granulocyte/macrophage colony stimulating factor (GM-CSF)[109]. This

cytokine was recently shown to promote the growth, invasion, and metastatic potential of

pancreatic cancer cells[110]. Other cytokines that could activate IL2RG-mediated signaling include

IL-4, which has been reported to enhance proliferation of several IL-4RA-expressing human pancreatic cancer cell lines[111], although evidence pointed to signaling occurring through an alternative receptor complex. This study is also at odds with our observation that Il2rg is not expressed *in vitro* by pancreatic cancer cell lines.

Coreceptors of IL2RG have been successfully targeted in other cancer types.[112][113] Our results raise the possibility that there could be value in targeting this pathway therapeutically. There are JAK3 inhibitors in use in the clinic for the treatment of rheumatoid arthritis (PMID25047498). Thus, a JAK3-specific inhibitor such as Tofacitinib that could inhibit the growth of IL2RG-expressing pancreatic cancer cells could potentially have efficacy in patients. Tofacitinib has been reported to reduce cancer growth in xenograft models of human T-cell lymphoma[114].

Early studies suggested that other JAK inhibitors might have a role in treating pancreatic cancer[115, 116]. However, a phase 3 clinical trial using Ruxolitinib, a JAK1 inhibitor, for patients with advanced pancreatic cancer was recently terminated due to disappointing efficacy[117]. Clinical trials for Momelotinib, a JAK1/2 inhibitor, in combination with Gemcitabine and Nab-paclitaxel are ongoing (https://clinicaltrials.gov/show/NCT02101021). Notably, these clinical trials were undertaken to determine the efficacy of using this momelotinib to target immune cells in the cancer microenvironment, not pancreatic cancer cells themselves. In canonical Il2rg signaling, JAK1 dimerizes with JAK3 immediately downstream of the receptor. It is possible that these inhibitors may inhibit Il2rg signaling in cancers expressing it.

Beyond the possibility of chemotherapeutic targeting, IL2RG expression may hold implications for pancreatic cancer immunotherapy[118]. Researchers are exploring the use of administered cytokines, both alone and in conjunction with vaccines, to stimulate activation and responsiveness in immune cells to help overcome immunosuppressive influences within the

tumor microenvironment. Clinical studies of preoperative administration of IL-2 have shown increases in survival and progression free survival of pancreatic cancer patients[119, 120]. Systemic IL-2 is being used in an ongoing clinical trial for a vaccine targeting P53 + Ras (NCT00019084 and previous, now suspended trial for a vaccine targeting CEA (NCT01723306). Although these trials have been focused on stimulating vaccine response, it is possible that IL-2 could stimulate proliferation of cancers expressing Il2rg.

In conclusion, we find that IL2RG is expressed at the earliest stages of pancreatic cancer with a significant role in tumorigenesis. Further study is required to elucidate its precise mechanism of action and potential as a therapeutic target. Of particular interest would be identifying which (if any) of the several possible ligands are stimulating IL2RG and if the pathway can be replicated *in vitro* by inducing IL2RG expression in pancreatic cancer cell lines.

Table 1. Highlighted transcripts differentially expressed between normal duct samples and PanIN3s.

ID	Log2 Fold Change	Average Expression	Adjusted p-value
REG4	-7.38599	5.30466	0.023446
FXYD3	-5.07836	5.840235	0.000135
WFDC2	-4.78364	5.183681	0.020943
ANXA10	-4.51085	5.467628	0.01682
IL2RG	-4.43129	3.516513	0.00111
MDK	-4.28123	4.562996	7.37E-05
CLDN18	-4.17368	7.513807	0.013711
TXNIP	-4.13336	6.549126	0.003369
CTSE	-4.00825	8.741542	0.049768
PPARG	-3.97045	3.8431	2.11E-06
MECOM	-3.76696	4.570754	3.75E-05
NQO1	-2.45764	5.339688	0.001632
IDH1	-2.40941	4.138584	0.008271
TIMP1	-1.55919	6.426763	0.01714
CDKN1A	2.359616	5.176117	0.033195
TFPI2	3.676845	1.258874	9.62E-06
RELN	3.994777	1.305201	0.000128
SPP1	4.38009	3.243471	0.02906
CFTR	4.464813	4.610521	0.060118

Table 2. Transcripts overexpressed in PanIN3s (exclusively among PanINs) vs normal duct samples. These 50 transcripts had the lowest observed adjusted p-value of those in the comparison.

ID	Log 2Fold Change	Average Expression	Adjusted p-value
RRM2	-1.9140	1.4590	0.0007
COTL1	-1.9507	1.7187	0.0010
DLEU7	-4.4313	3.5165	0.0011
CDHR2	-2.9820	1.5269	0.0024
PTK6	-1.5232	0.9612	0.0027
PSMC1P2	-2.9991	1.8893	0.0029
SDR16C5	-3.2507	2.3845	0.0029
CFL1P5	-0.9414	0.8916	0.0035
SFT2D2	-1.9217	3.2840	0.0045
LGR4	-2.2449	4.7128	0.0045
HIST2H2AA3	-2.0518	3.2689	0.0062
OR5M11	-1.1188	1.5083	0.0072
TCF7L2	-1.4152	4.9378	0.0079
C4BPB	-3.0528	4.1796	0.0084
NAV1	-0.8635	4.2727	0.0091
IHH	-1.5999	2.3632	0.0094
ESRP1	-1.4203	2.8652	0.0106
SRD5A1	-2.1433	2.1493	0.0110
INCENP	-1.1449	2.2765	0.0112

KIF18B	-1.2251	1.2764	0.0118
REXO2	-2.0702	2.1871	0.0125
C10orf10	-2.5738	2.3101	0.0140
NFE2L1	-0.7765	2.1765	0.0142
PARP3	-1.5804	2.6449	0.0142
B3GNTL1	-1.2879	2.9137	0.0147
AP2M1	-0.7532	0.7778	0.0150
CST1	-1.0883	2.9051	0.0153
UBE2C	-0.9914	1.9686	0.0155
ZDHHC9	-1.4257	2.2199	0.0155
HOXB7	-0.9832	4.9748	0.0158
EZH2	-0.7633	1.2502	0.0159
LRRC31	-1.0461	2.9554	0.0164
PI3	-4.5108	5.4676	0.0168
PNMA1	-1.0149	0.6347	0.0170
PGM2L1	-1.8820	2.7490	0.0174
PSMB5	-1.3387	1.6433	0.0178
OASL	-0.9336	1.6202	0.0183
HIST1H2AI	-2.1301	2.2790	0.0189
SEC16B	-0.7911	0.5556	0.0190
CIT	-0.7100	1.9789	0.0192
GPI	-0.6109	0.6424	0.0202
FAM162A	-1.9028	3.7472	0.0204
IGF2BP3	-0.9323	2.4589	0.0209
FER1L4	-2.5120	4.1109	0.0209
ADCY7	-1.4517	3.0690	0.0211

MYBL2	-1.5384	2.6855	0.0214
CCNG2	-2.1469	2.6027	0.0218
GRN	-1.5119	2.3488	0.0221
DAPP1	-0.9239	3.9139	0.0223
FSCN1	-1.5080	2.3276	0.0223

Table 3. Transcripts overexpressed in collective PanINs (1s, 2s, 3s) vs normal duct samples.
These 50 transcripts had the lowest observed adjusted p-value of those in the comparison.

ID	log2 Fold Change	Average Expression	Adjusted p-value
LIN7A	0.8230	0.7511	0.0004
MTUS2	0.7124	0.6129	0.0004
LYPD6B	2.0132	4.0781	0.0004
C3orf45	1.2850	1.1219	0.0004
GUCA2A	1.0463	0.7278	0.0004
NOSTRIN	1.2269	3.9486	0.0004
AKAP7	1.0568	1.5492	0.0004
VGLL1	1.1566	0.9448	0.0004
STEAP4	1.6482	1.6987	0.0004
SOX6	0.9508	1.5692	0.0005
DTNA	0.9268	0.7952	0.0005
CCDC141	0.5392	0.5739	0.0008
CALN1	0.5788	0.5917	0.0008
CADM1	1.0328	1.1690	0.0008
GABRA5	0.6764	0.5324	0.0010
LRRC7	0.6799	0.5073	0.0010
SLC2A2	2.3039	1.8808	0.0010
SLCO4C1	0.9252	0.8117	0.0011
NRP1	1.1469	2.3269	0.0016

CNR1	0.5538	0.5364	0.0017
TGFB2	1.6434	1.4661	0.0018
GPR64	1.3701	1.7352	0.0018
MTUS2-AS1	0.7541	0.5469	0.0018
POU6F2	1.1592	0.9124	0.0018
DSCAML1	1.0114	0.7466	0.0018
NR1H4	1.4736	1.1337	0.0022
NUCB2	2.0968	2.7005	0.0022
METTL7A	1.0773	3.1398	0.0025
NME5	1.3781	1.6224	0.0025
ALDH1A2	0.8765	0.7939	0.0025
VEPH1	0.7521	0.7368	0.0028
ZNF704	0.7882	2.4856	0.0028
ZNF135	0.6310	0.6585	0.0028
EFEMP1	1.6396	1.6833	0.0028
GLIS3	2.3102	2.9767	0.0029
WNK2	0.7345	0.8225	0.0033
RALYL	1.6245	1.2176	0.0039
SETBP1	0.9642	1.5749	0.0039
TTLL7	1.4302	1.6411	0.0044
CASP9	0.9464	1.7125	0.0044
ZFP36L2	1.0260	6.2748	0.0044
BCO2	1.3985	1.3799	0.0047
TMEM27	0.7675	0.8127	0.0049

SLC9A3R2	1.3708	2.3320	0.0049
DDIT4	5.3228	4.3957	0.0050
HYDIN	0.5354	0.5834	0.0050
DYRK3	0.8975	1.2922	0.0051
BCL2	0.7139	1.0227	0.0054
BEX5	2.3786	2.1284	0.0057
CTNND2	1.1492	0.8584	0.0057

Table 4. Transcripts underexpressed in PanIN3s vs. normal duct samples. These 50
transcripts had the lowest observed adjusted p-value of those in the comparison.

ID	log2 Fold Change	Average Expression	Adjusted p-value
VGLL1	3.4168	0.9448	1.38E-08
AKAP7	2.9597	1.5492	1.38E-08
GUCA2A	2.8986	0.7278	1.38E-08
LIN7A	2.2845	0.7511	1.38E-08
GABRA5	2.0514	0.5324	1.38E-08
MTUS2	1.9404	0.6129	1.38E-08
CALN1	1.7263	0.5917	1.38E-08
CCDC141	1.5185	0.5739	2.21E-08
CNR1	1.6342	0.5364	5.05E-08
LRRC7	1.8733	0.5073	6.20E-08
SLCO4C1	2.5472	0.8117	6.86E-08
DOK5	3.3269	1.0830	8.84E-08
POU6F2	3.2967	0.9124	8.84E-08
ALDH1A2	2.6025	0.7939	8.84E-08
TMEM27	2.4447	0.8127	8.84E-08
STEAP4	3.8134	1.6987	1.25E-07
MTUS2-AS1	2.0858	0.5469	1.25E-07
DTNA	2.1122	0.7952	2.52E-07
C3orf45	2.6853	1.1219	3.05E-07
APOH	1.7932	0.5537	8.04E-07

NOV	3.4220	1.2958	8.12E-07
NOSTRIN	2.3365	3.9486	8.26E-07
VEPH1	1.9311	0.7368	8.75E-07
SLC17A4	4.2270	1.6212	1.19E-06
EFEMP1	4.0484	1.6833	1.48E-06
BCO2	3.6607	1.3799	1.53E-06
ATP10A	1.6310	0.7804	1.57E-06
KIAA0319	1.7509	0.7370	1.73E-06
WNK2	1.8183	0.8225	1.86E-06
KRT4	1.2670	0.5602	1.86E-06
DSCAML1	2.2920	0.7466	2.20E-06
PAH	3.3364	0.8778	2.24E-06
NR1H4	3.3489	1.1337	2.61E-06
SOX6	1.8174	1.5692	2.80E-06
CYP39A1	1.1183	0.5530	2.93E-06
CNTN4	1.5465	0.7198	3.15E-06
SIM1	1.9766	0.6375	3.41E-06
SETBP1	2.2357	1.5749	5.57E-06
HYDIN	1.2654	0.5834	6.74E-06
KCNMA1	2.2177	0.8478	8.51E-06
ANGPT1	1.4105	0.6487	8.51E-06
BCL2	1.6681	1.0227	8.80E-06
APCDD1	4.9079	2.4655	8.93E-06
CYS1	2.3736	0.9061	8.93E-06
NRP1	2.2758	2.3269	8.93E-06

SERPINA 6	3.3514	1.5053	9.36E-06
TFPI2	3.6768	1.2589	9.62E-06
C8orf42	2.9061	1.2862	9.70E-06
GRM8	0.9407	0.4561	1.08E-05
CDKN1C	2.7625	1.4192	1.22E-05
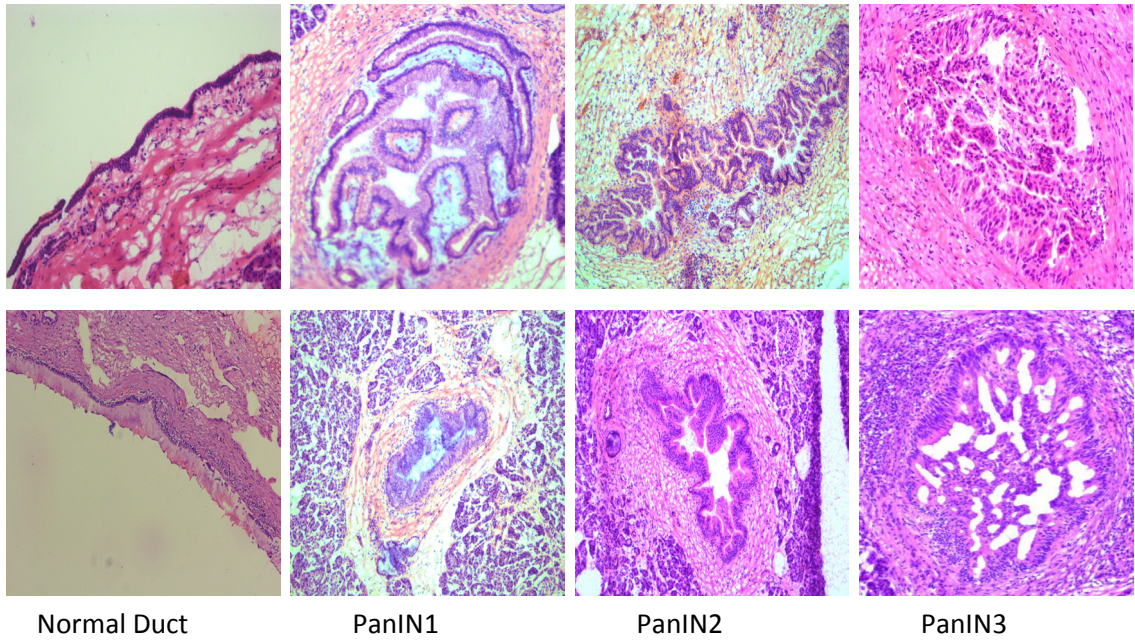
Figure 1. Example pancreatic lesions dissected for RNA. All slides were stained with Hemotoxylin and Eosin and photographed at 4x magnification.
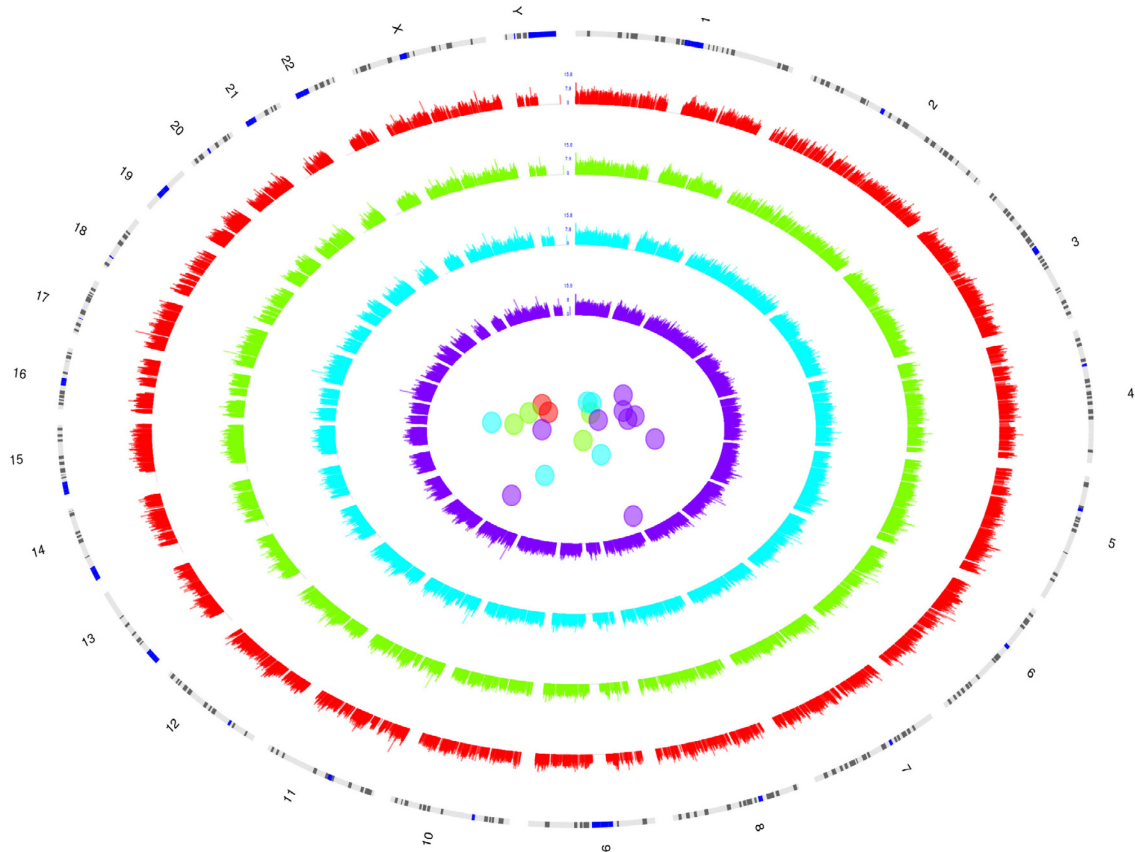
Figure 2. Circos and PCA plot of normal and PanIN samples. Red = normals, green = PanIN1s, blue = PanIN2s, purple = PanIN3s. Each grade of samples shows greater divergence in transcript expression than the last from normal and other samples of the same grade. Of the 9 PanIN3 samples, 4 are highly-clustered and 3 are drastic outliers.
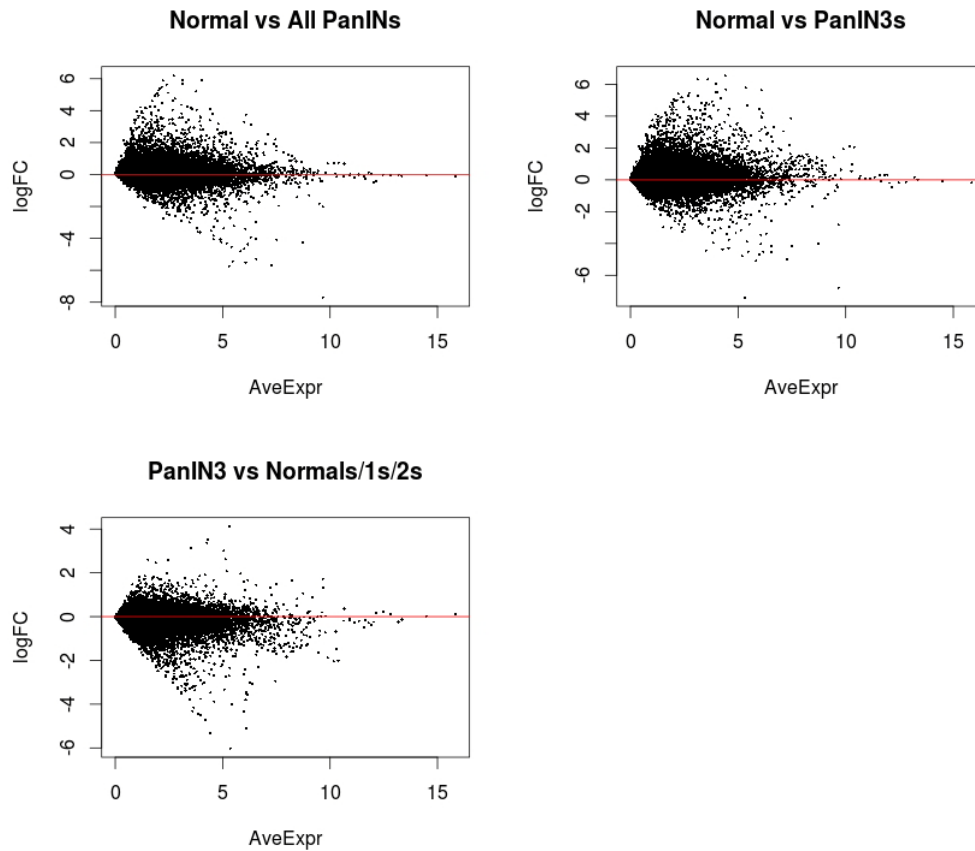
Figure 3. MA plots of differential expression comparisons. Each dot represents a gene. Interestingly, PanIN3s trend more towards underexpressing a greater number of genes in comparison to normal ducts and other PanINs than overexpressing.

REG4

PanIN1   PanIN3   PDAC
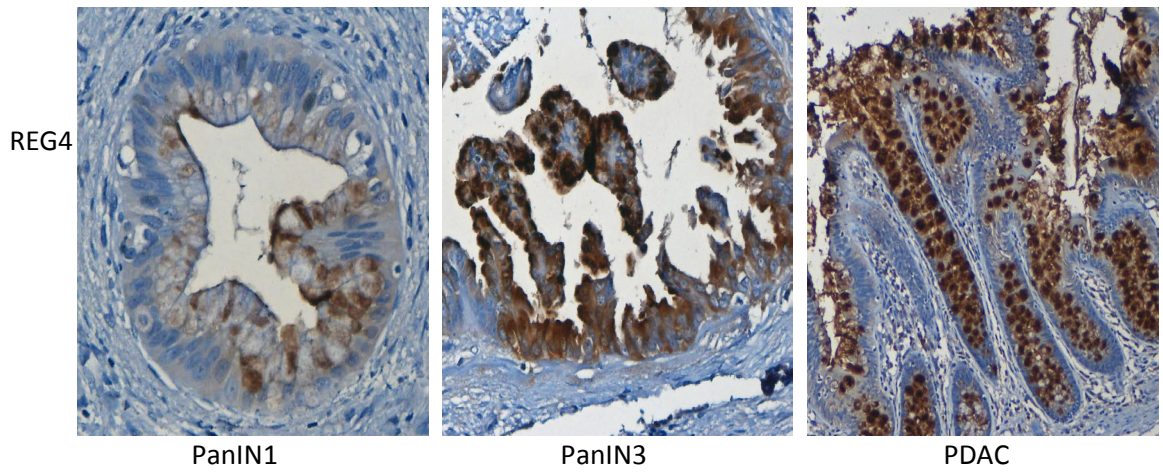
Figure 4. Immunohistochemical analysis of REG4 expression in pancreatic lesions. PanIN1 lesions have weak labeling of REG4. PanIN3 and PDAC lesions have strong labeling of REG4.

A

B

Log 2 T P M

Log 2 T P M

Normal Duct   PanIN1   PanIN2   PanIN3

IL2RG   PTPRC   CD3D

C JAK-STAT SIGNALING PATHWAY

-1   0   1

Endocytosis

Lysosomal proteolysis

Ubiquitin mediated proteolysis

Cbl   +u   +u   SOCS

EPO
IFN/IL10
IL2G
IL6
UPD

Cytokine

Cytokine-cytokine receptor interaction

STAM

Cytokine   JAK   -p   +p   STAT   Homo/ hetero STAT dimers

SHP1   PIAS   STAT 5

IFNα
P48

Pim-1

CBP

CIS

Growth, proliferation, fate determination, development, immunity

c-Myc
CycD

Cell cycle

+p   SHP2   GRB   SOS   Ras/ MAPK   MAPK signaling pathway

BclXL   Antiapoptosis

Spred   Apoptosis
Sprouty

+p   PI3K   +p   AKT   Antiapoptosis

PI3K-Akt signaling pathway   Apoptosis

Data on KEGG graph
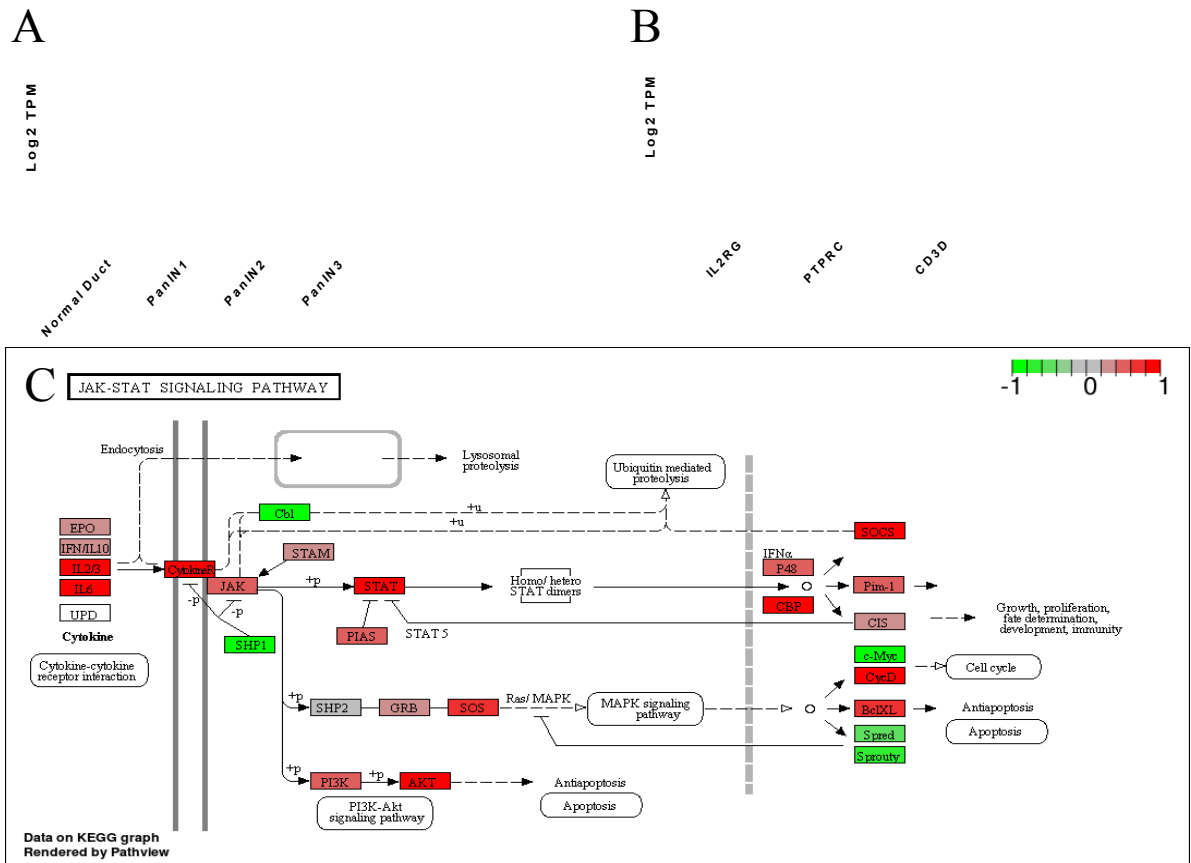Rendered by Pathview

Figure 5. IL2RG mRNA expression in PanINs. (a) IL2RG mRNA expression was assessed with limma and transcript per million (TPM) values were averaged for each PanIN grade. (b) mRNA expression of PTPRC and CD3D, two lymphocytic markers used here to assess immune infiltration, did not increase in higher-grade PanINs. (c) The results of the differential comparison analysis of normal duct and PanIN3 samples were overlaid on the KEGG JAK-STAT pathway using Gage and Pathview Bioconductor tools. Several additional genes interacting with or targeted by the IL2RG signaling pathway are differentially expressed. Red = overexpressed in PanIN3s (adjusted p-value < 0.1), green = underexpressed in PanIN3s relative to normal duct (adjusted p-value < 0.1).

IL2RG

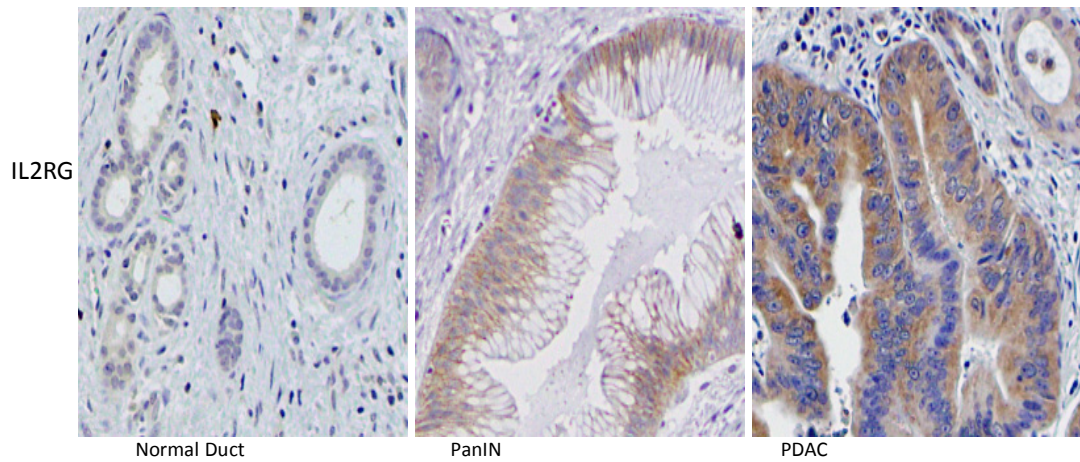Normal Duct   PanIN   PDAC

Figure 6. Immunohistochemical analysis of IL2RG expression in tissue microarrays.
Normal pancreatic ducts have weak or negative labeling of IL2RG. PanIN and PDAC lesions
have moderate or strong labeling of IL2RG. Note the expression of IL2RG in immune cells in
the stroma.
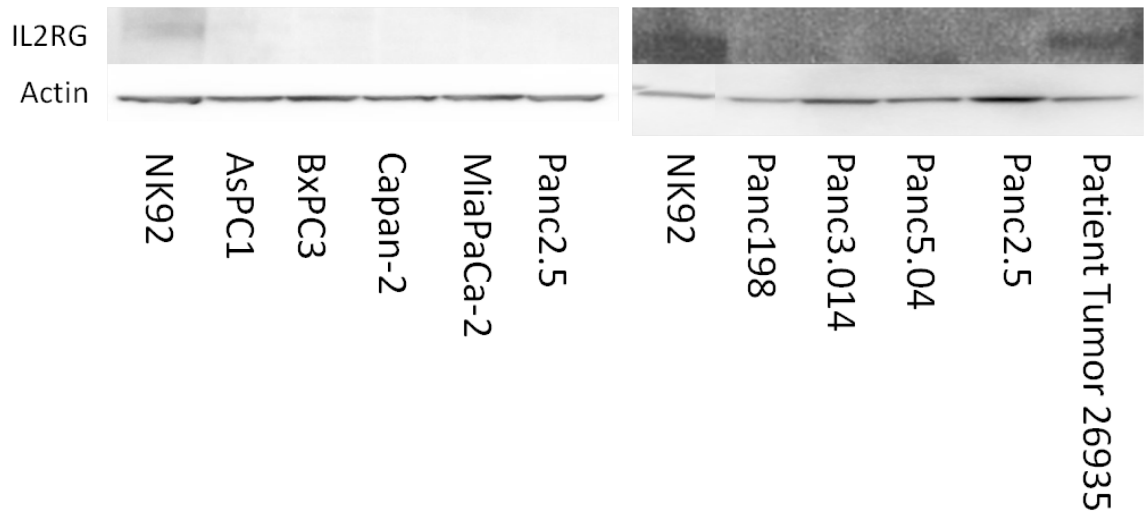
Figure 7. Western blot analysis of IL2RG protein levels in pancreatic cancer cell lines. NK-92, a natural killer cell line, and patient tumor 26935 are positive for IL2RG expression. All tested PDAC cell lines are negative for IL2RG expression.

A

IL2RG

Normal Duct   PanIN   PDAC

B

IL2RG
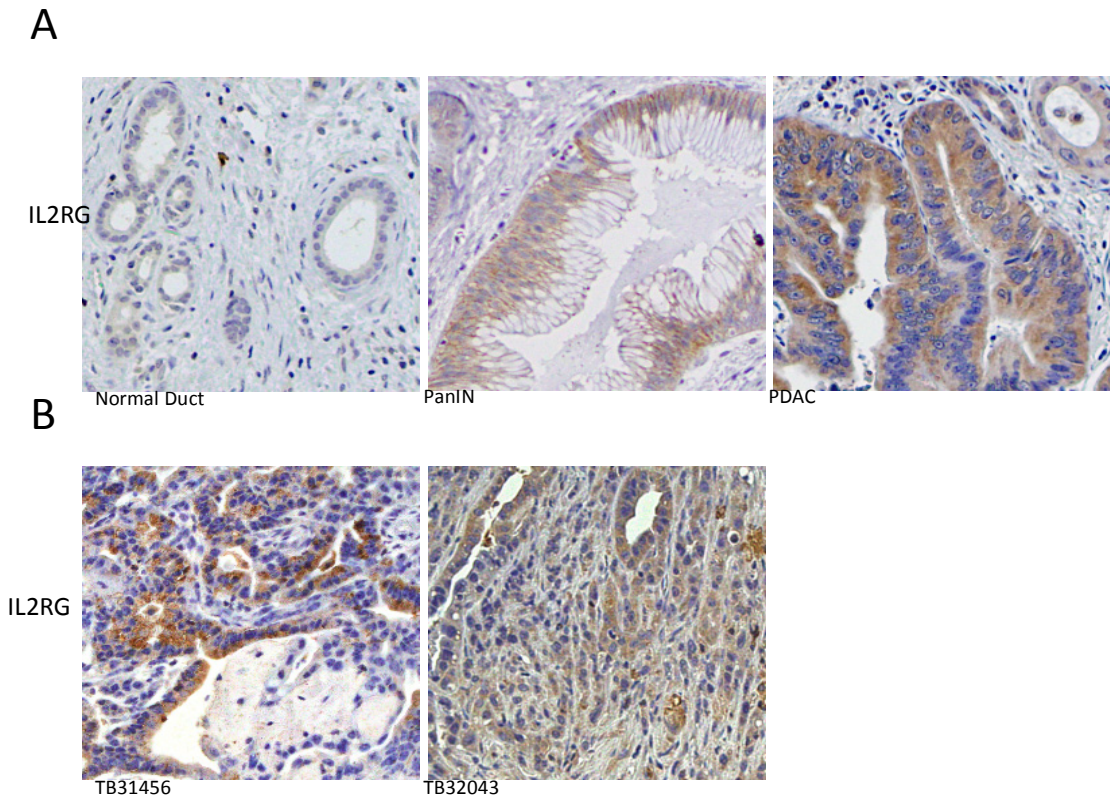
TB31456   TB32043

Figure 8. Immunohistochemical analysis of IL2RG expression. A) Human tissue pancreatic microarrays. Normal ducts do not label, PanINs label weakly, and PDAC labels intensely. B) Mouse xenografts. TB31456 and TB32043 label positive for IL2RG in vivo.
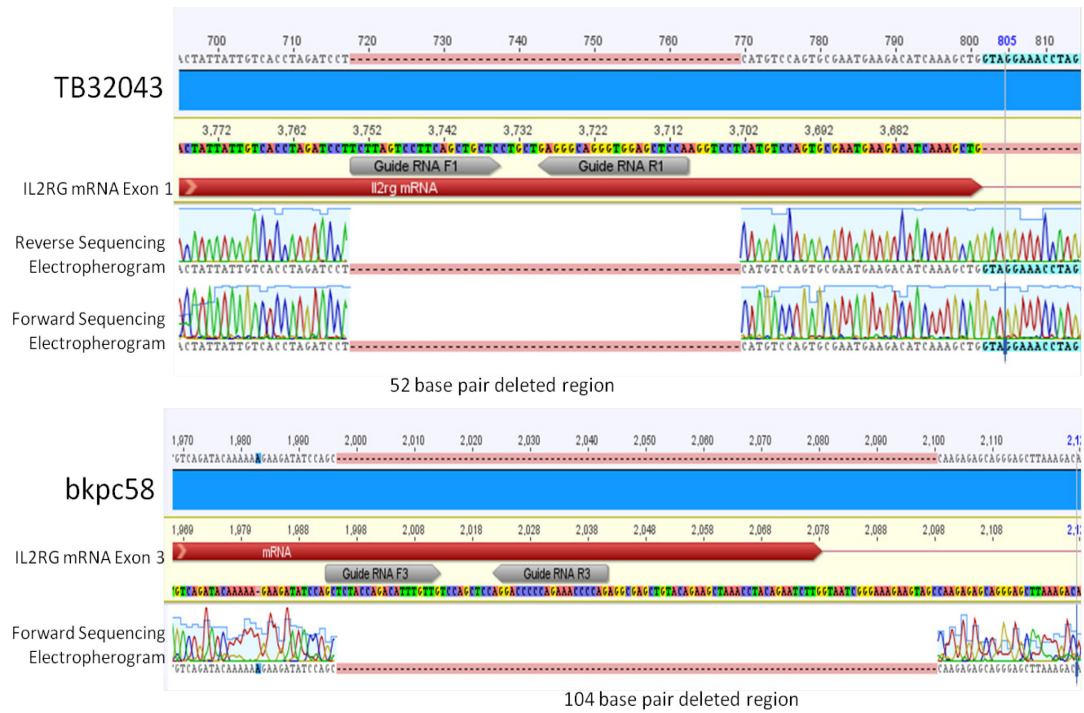
Figure 9. Electropherograms of IL2RG CRISPR-deleted regions in mouse cell lines. A) TB32043 is a female line with a biallelic 52 base pair deletion in exon 1 of IL2RG. B) bkpc58 is a male line with a 104 base pair deletion in exon 3 of IL2RG.
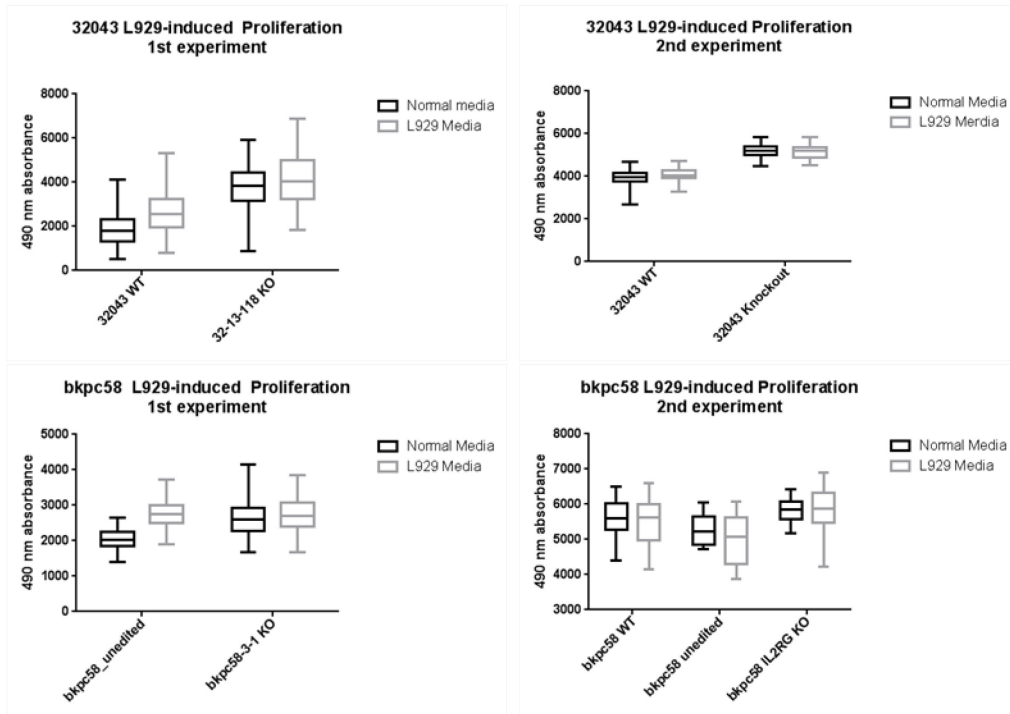
Figure 10. L929-induced proliferation of IL2RG knockout mouse pancreatic cancer cells. Cells were treated with L929-conditioned media for 72 hours and then assayed for metabolically active cells using AlamarBlue. Although a significant induction of proliferation was observed in the wild type cells (and not IL2RG knockout cells) of some experiments, this result proved inconsistent in replicate experiments.
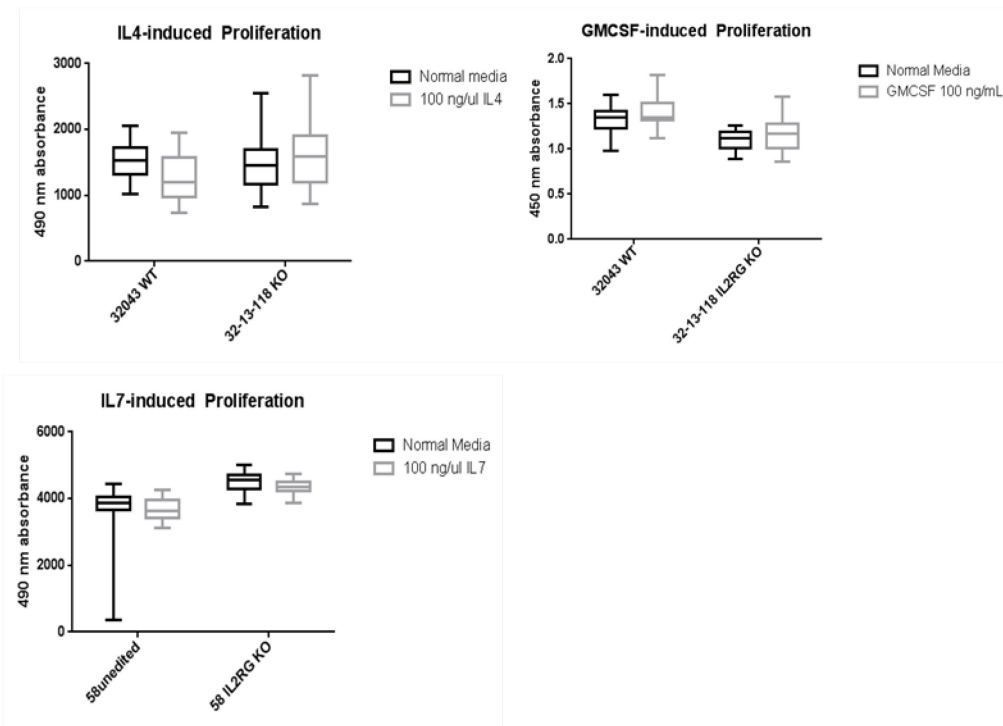
Figure 11. IL2RG ligand induced proliferation in IL2RG knockout mouse pancreatic cancer cells. Cells were treated with 100 ng/ul of one IL2RG ligand: IL-4, GM-CSF, or IL-7. After 3 days, proliferation was measured using AlamarBlue to assay for metabolically active cells. None of the ligands induced significant proliferation in wild type or IL2RG knockout cells.
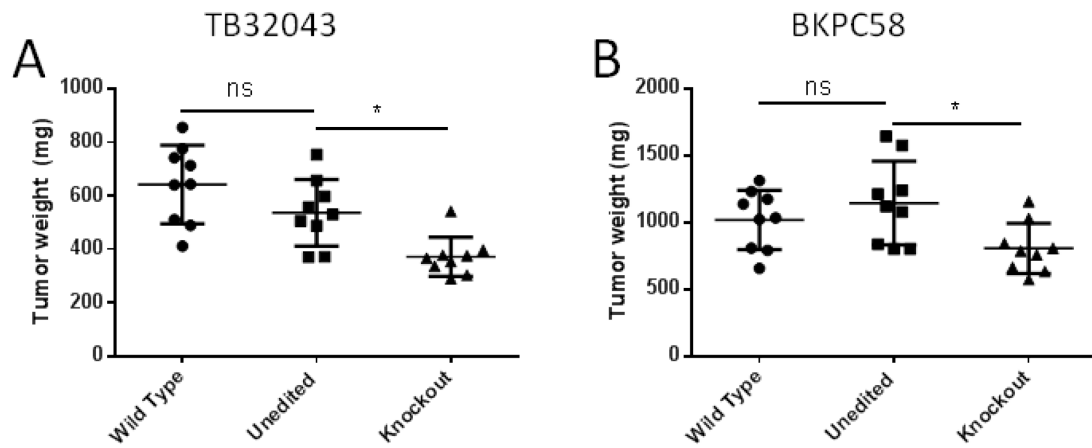
Figure 12. Phenotype of IL2RG CRISPR-edited xenografts. There is no significant difference in the tumor weight of the wild type and CRISPR-treated (but unedited) xenografted A) TB32043 and B) bkpc58 cells. In contrast, A) TB32043 and B) bkpc58 cells with IL2RG knockout have significantly-reduced weight compared to unedited cells.
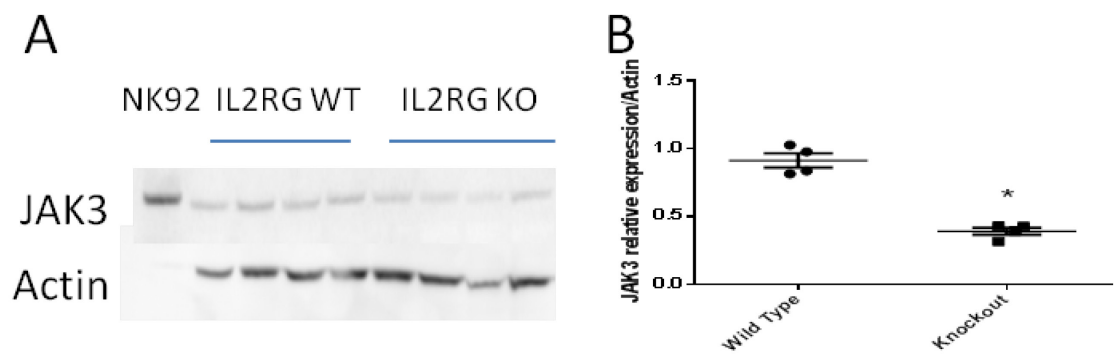
Figure 13. JAK3 expression in xenografted TB32043 cells. A) Xenografted IL2RG WT cells have significantly higher expression of JAK3 than IL2RG CRISPR-edited cells (NK-92 = human natural killer cells, + control). B) Quantification of JAK3/Actin expression in xenografted cancers.

Chapter 3. Neotranscription in PanINs

MATERIALS AND METHODS

Alternative Transcription Analysis

AltAnalyze (www.altanalyze.org) was run on BED files for RNA-sequencing data from 12 samples: 3 normal pancreatic duct and 9 PanIN3s. Species was set to human and the EnsMart65 database was used as a reference. The ASPIRE algorithm, described in detail in the AltAnalyze manual (http://www.altanalyze.org/help_main.htm , section 3.2), was used to score exon inclusion/exclusion events. In brief, a ratio is calculated separately for the inclusion and exclusion of a reciprocal junction, in which expression of the junction is divided by the mean of all gene expression reporting junctions and exons. The experimental group (PanIN3) vs. control (normal duct) ratios were then calculated, along with a false-discovery rate p-value (Benjamin-Hochberg correction). Lineage Analysis was performed by calculating correlation coefficients of the sample groups to Lineage WikiPathways networks.

RT-PCR

To examine levels of alternatively spliced transcripts in PDAC, RNA was harvested from pancreatic cancer cell lines and pancreatic cancer patient tumor samples. 1 μg total RNA from each sample was reverse transcribed using QuantiTect Reverse Transcription Kit (Qiagen) according to the manufacturer's protocol. The resulting cDNA was diluted 1:200 on the ABI 7300 Real-Time PCR thermocycler (Applied Biosystems) using SYBR Green PCR Master Mix and recommended PCR conditions (Applied Biosystems). Melting curve analysis and normalization to 18S rRNA was performed.

Primers were designed to target isoform-specific regions of MUC1, ANXA2, and MYO10 and ordered from Integrated DNA Technologies (www.idtdna.com):

ANXA2 Normal Isoform F1 5'- CCAGGGTGAAAATGTTTGCCA

ANXA2 Normal Isoform R1 5'- GCTTGCACAGGATTTCGTGA

ANXA2 PanIN3 Isoform F1 5'- GGCTGCCCACTTCCTTCAAA

ANXA2 PanIN3 Isoform R1 5'- TCCCGCTCAGCATCAAAGTT

MUC1 Normal Isoform Exon5-6 F1 5'- AGCGTGAGTGATGTGCCATT

MUC1 PanIN3 Isoform Exon5-6 F1 5'- TCAGCGGCTGTCTGTCAGT

MUC1 Isoform-Agnostic Exon5-6 R1 5'- CGCCCATGGGTGTGGTAG

MYO10 Full Isoform F1 5'- GATAACTTCTTCACCGAGGGAACA

MYO10 Full Isoform R1 5'- CCGGCTGTACTGCTCCATGGTGGCAG

MYO10 Headless Isoform F1 5'- CAGCACAGCCCGAGACGCAC

MYO10 Headless Isoform R1 5'- CTTGGGTTTTCTTTCACCCCTTCAG

RNA in situ hybridization

Proprietary probes targeting bases 1262-2318 of the NM_012334.2 transcript sequence for fMYO10 were designed and manufactured by Advanced Cell Diagnostics (www.acdbio.com). RNAscope assay was performed according to the manufacturer's protocol with the 2.0 HD RED Assay on tissue microarrays (TMAs) of pancreatic normal and cancer spots. A total of at least 1000 cells were examined from each group and red staining foci were counted. Foci were normalized to the number of cells counted from each group.

shRNA inhibition of MYO10 isoforms

Hairpin shRNA sequences targeting isoform-specific regions of MYO10 were designed with the Oligoengine software (www.oligoengine.com) and ordered from Integrated DNA Technologies (www.idtdna.com):

Fusion detection analysis

BED files from 8 samples (2 normal duct, 2 PanIN1, 2 PanIN2, 2 PanIN3) were analyzed with Tophat-fusion (http://ccb.jhu.edu/software/tophat/fusion_index.shtml). The fusion minimum distance was set to 100000000 and anchor length to 13. Tophat-fusion-post results were further filtered using Oncofuse (www.unav.es/genetica/**oncofuse**.html). Finally, events meeting any of the following criteria were filtered out:

1. Fusion event reported in normal sample

2. Fusion event includes a gene and partnered pseudogene.

3. Fusion partners are not in parallel or coding orientation.

RESULTS

The AltAnalyze lineage profiler compares sample expression data to a database of tissue-specific lineage profiles of transcription markers generated by AltAnalyze from public Affymetrix and GEO repositories of Affymetrix Exon 1.0 data. We performed this analysis on our samples. The pattern of isoform expression in our normal duct samples correlated very strongly with the pancreas lineage profile and little else.   The isoforms expressed in our PanIN1 samples correlated most-strongly with the pancreas lineage profile, but had positive Z scores for a few other tissues. Isoform expression in both PanIN2 and PanIN3 samples showed little correlation to the pancreas lineage profile and much stronger correlations to the lineage profile of several other tissues, including colon, fetal large intestine, and fetal small intestine.

We compared the transcriptional profiles of PanIN3 and normal duct samples. We generated a list of 3053 exon inclusion events mapping to known genes. We did not observe a reduction in splicing diversity that had been reported in pancreatic cancer cell lines[79]. 1200 of the 3053 events were predicted to result in a downregulation of the corresponding isoform in PanIN3s and 1853 were predicted to result in an upregulation.

Many of the alternatively spliced transcripts were of unknown biological significance, but a few stood out based on literature review and were selected for follow up (Table 2). The MUC1 gene possesses a variable number of tandem repeats (VNTR) region and has 20 amino acids subject to variable O-glycosylation. In over 80% of pancreatic adenocarcinomas MUC1 is differentially glycosylated which can affect the chemosensitivity of cancer[121]. In our list of candidate alternatively spliced transcripts, two of the highest scored (-0.82345, adjusted p-value = 0.00013 ;-0.74755, adjusted p-value = 0.00117) occur in MUC1. These splicing events map to an isoform previously described as oncogenic[122]. Annexin 2 (ANXA2) has several alternative splicing events, including one highly-scoring for inclusion in PanIN3s over normal ducts (-0.63655) that suggests a switch between two known isoforms. The functional significance of these isoforms is unknown, but ANXA2 is being investigated as a target for immunotherapy [123].

Three of the highest-scoring events (-0.75227, -0.72576, -0.72576) were for Myosin X (MYO10) transcripts, an unconventional myosin that acts to form filopodia on the cell surface (Berg, 2002). MYO10 has recently been established as playing an important role in cancer invasion and metastasis through construction of invadopedia, cell protrusions that are capable of penetrating and digesting extracellular matrix (Schoumacher 2010). MYO10 knockdown results in a considerable reduction of invadopedia formation and matrix digestion (Cao 2014). MYO10 overexpression promotes aggressiveness and metastasis in breast cancer, and its expression is induced in pancreatic cancer by the introduction of mutant p53 in mouse models [124, 125] . Silencing of MYO10 in breast and PDAC cells inhibits invasion[125].

MYO10 consists of two functionally-distinct isoforms, "full" (fMYO10) and "headless" (hMYO10). fMYO10 is connected to mitosis and cell migration in neurons, while hMYO10 is a dominant negative inhibitor of full[126]. The three splicing events reported correspond to inclusion of exons 18 and 19, which are part of the fMYO10 isoform. Counts of this inclusion event indicate that PanIN3s undergo a drastic alternative splicing event from a full : headless ratio of 7 : 42 in our normal duct samples to 56 : 7 in our PanIN3s. Notably, in our differential expression comparison, MYO10 fell short of the threshold for significance with an upregulation of 2.07-fold over the normal duct samples (Figure 4). Multiplying this fold-ratio by the calculated isoform ratio, PanIN3s upregulate fMYO10 by 16.57-fold over the normal ducts and downregulate hMYO10 by 3-fold.

We sought to corroborate our *in silico* findings through RT-PCR with isoform-specific primers for MUC1, ANXA2, and MYO10 (Figure 3). In all three genes, alternatively spliced isoforms implicated by our splicing analysis to be overexpressed in PanINs relative to normal pancreatic duct samples were also overexpressed in pancreatic cancer cell lines Panc5.04, MiaPaCa2, and Panc8.13 in comparison with the non-neoplastic pancreatic duct line HPDE. Both isoforms of MUC1 had comparable expression in pancreatic cancer cell lines, while for ANXA2 the normal isoform was proportionately more overexpressed than the PanIN isoform. With MYO10, we saw much greater overexpression of the full, putatively oncogenic, isoform than the headless isoform in pancreatic cancer cell lines in comparison to HPDE.

MYO10

In order to confirm the cellular source of MYO10 isoform transcripts, we performed RNA in situ hybridization on tissue microarrays containing PDAC and normal pancreas tissues with probes targeting isoform-specific regions of fMYO10. Primary pancreatic cancer cells had a significantly greater number of stained foci than normal duct cells, though the difference was

much smaller than determined by RNA-seq data: Normal duct: 248 foci in 1243 cells (0.20 foci/cell); pancreatic cancer: 445 foci in 1003 cells (0.44 foci/cell) (Figure 4).

No isoform-specific antibody is commercially available for MYO10, but the two major isoforms are distinct enough in size (hMYO10 = 165 kDa, full = 240 kDa) to distinguish by western blot. The 6 cell lines (1 normal, 5 cancer) and the two patient PDAC samples tested all expressed hMYO10. 2 of the 5 cancer lines additionally expressed fMYO10. Interestingly, Panc8.13 expressed a truncated isoform consistent with the known MYO10 frameshift insertion mutation in this cell lines[17].

Functional role of fMYO10 in cell lines

To determine the functional impact of the specific MYO10 isoforms in pancreatic cancer cells, we treated MiaPaCa2 cells with shRNA constructs targeting isoform-specific regions of the gene. Expression of fMYO10 was successfully inhibited in MiaPaCa2 cells (Figure 6). Previous studies have indicated a critical role for MYO10 in filopodia formation. Wild type MiaPaCa2 and fMYO10 knockout MiaPaCa2 cells were stained and imaged by fluorescent microscopy for differences in filopodial phenotype. We found no qualitative difference (Figure 7A).

MYO10 has also been linked to invasiveness in cancer[125]. We performed a wound healing assay on wild type and knockout cells to compare their motility. No difference was observed in the rate of wound healing between these cell types (Figure 7B).

Fusion transcripts in PanINs

Our fusion detection analysis was performed on the 8 samples (2 normal, and 2 from each PanIN grade) sequenced on the Illumina platform due to their higher read length. Candidate fusion events were filtered out using the Oncofuse tool and manual inspection, using the following criteria:

1. Fusion event reported in normal sample

2. Fusion event includes a gene and partnered pseudogene.

3. Fusion partners are not in parallel or coding orientation.

This reduced the list to 16 candidate fusion transcripts (Table 3), each of which was only detected in one PanIN sample. The frame difference between partners of each event is included. It is unlikely that frame differences other than 0 produce a functional transcript, though they may still be real chromosomal rearrangements. For six of these events, one or both fusion partners has been previously reported in human cancer, although none of them have been reported in a pancreatic cancer[81]. These partners include: HINT1, TJP1, DNM2, LARGE, MLLT10, PP2R1B, and FTFT1. A few of the partners have promising roles. The region of DNM2 included in one fusion contains miRNA199-a, which is oncogenic in pancreatic cancer[127]. HINT1 has been described as having tumor suppressor functions in certain contexts[128, 129]. We detect a HINT1-NECAP2 fusion in which HINT1 has a frameshift of 2 base pairs, possibly resulting in its inactivation. NECAP2 has been recently tied to EGFR endocytosis in breast cancer[130].

DISCUSSION

We identify several alternatively spliced transcripts in PanINs that may be of biological significance: Annexin 2 is being investigated as an antigenic target for immunotherapy [123]. Mucins play a major part in some of the most threatening aspects of pancreatic cancer: therapeutic resistance, invasiveness, and metastasis[131]. Mucin 1 is known to be upregulated as early as in low grade PanINs and has a role in tumorigenesis[132].

While two previous studies have reported oncogenic MYO10 overexpression in breast and pancreatic cancer[124, 125], MYO10 overexpression in PanINs was only modest (2.07-fold

upregulated in PanIN3s relative to normal duct, q=0.0029), if the expression of alternate transcripts was not accounted for. In PanINs and in pancreatic cancer cell lines, the distribution of isoforms has dramatically changed from primarily hMYO10 to primarily fMYO10.   However, we did not observe a phenotypic difference (qualitative filopodia density or cell migration) between parental pancreatic cancer cells expressing fMYO10 to knockdown cells.

Using fusion analysis, we also report on 16 *in silico* fusion transcripts occurring in our six PanIN samples that may produce chimeric mRNAs. None of these transcripts were recurrent in multiple PanINs. Unfortunately, there was not sufficient RNA from these PanINs to perform a confirmatory RT-PCR. Nevertheless, several of the 16 include partners previously identified as belonging to oncogenic fusion events in other cancers.

Table 5. Gene fusion events in PanIN samples

PanIN Grade	Sample Name	Genomic Coordinates	5' Partner	In CDS?	Segment Type	AAs	3' Partner	In CDS?	Segment Type	AAs	Frame Difference
PanIN1	9797_A	chr11:124618285>chr5:130495303	VSIG2	Yes	Intron	283	HINT1	Yes	Exon	55	2
PanIN2	12471_B	chr15:29992583>chr1:150444942	TJP1	No	Exon	1749	RPRD2	Yes	Exon	290	2
PanIN3	43581	chr1:28948520>chr19:10919344	TAF12	Yes	Exon	24	DNM2	Yes	Intron	352	0
PanIN3	13047_A	chr12:112466895>chr22:34286192	NAA25	No	Exon	973	LARGE	No	Intron	757	0
PanIN1	9033_B	chr6:34613650>chr10:21849200	C6orf106	Yes	Intron	170	MLLT10	Yes	Intron	989	1
PanIN3	13047_A	chr11:111601277>chr8:11695904	PPP2R1B	Yes	Intron	637	FDFT1	Yes	Exon	72	2
PanIN3	13047_A	chr3:115762921>chr1:207504497	LSAMP	Yes	Intron	129	CD55	Yes	Exon	205	1
PanIN3	43581	chr20:30789723>chr20:30388770	PLAGL2	Yes	Exon	85	TPX2	Yes	Intron	37	2
PanIN3	13047_A	chr3:132286286>chr7:152040114	ACAD11	Yes	Intron	667	KMT2C	Yes	Intron	4829	2
PanIN3	13047_A	chr1:75172003>chr1:16770125	CRYZ	Yes	Exon	321	NECAP2	Yes	Intron	244	0
PanIN3	13047_A	chr17:60129896>chr10:71913723	MED13	Yes	Intron	156	SAR1A	Yes	Exon	83	1
PanIN3	43581	chr13:108870882>chr13:108863645	ABHD13	No	Exon	0	LIG4	No	Intron	912	0
PanIN1	9033_B	chr9:5973893>chr2:168908148	KIAA2026	Yes	Intron	264	STK39	Yes	Intron	88	0
PanIN3	43581	chr1:209807838>chr1:55337263	LAMB3	Yes	Exon	172	DHCR24	Yes	Exon	306	2
PanIN3	43581	chr4:54439789>chr4:72306332	LNX1	Yes	Intron	126	SLC4A4	Yes	Intron	826	2
PanIN1	9797_A	chr3:134204574>chr3:134225976	ANAPC13	No	Exon	0	CEP63	Yes	Exon	681	0

Figure 14. Normal duct lineage profile. The isoform expression pattern in normal epithelium samples matches only the Pancreas profile in the AltAnalyze lineage database.
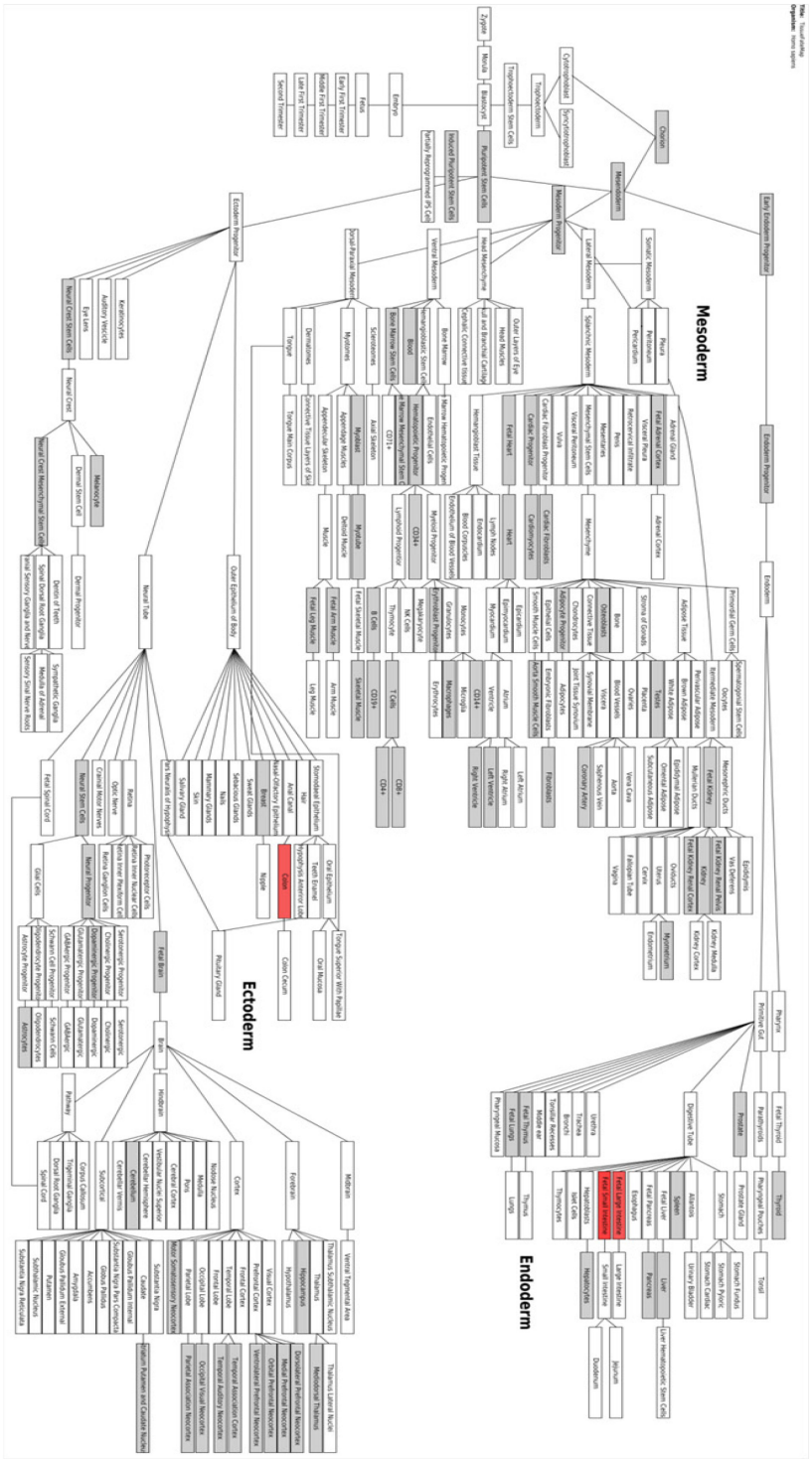
Figure 15. PanIN lineage profile. The isoform expression patterns in PanIN samples matches the colon, fetal large intestine, and fetal small intestine profiles, but not the pancreas profile in the lineage database.

59
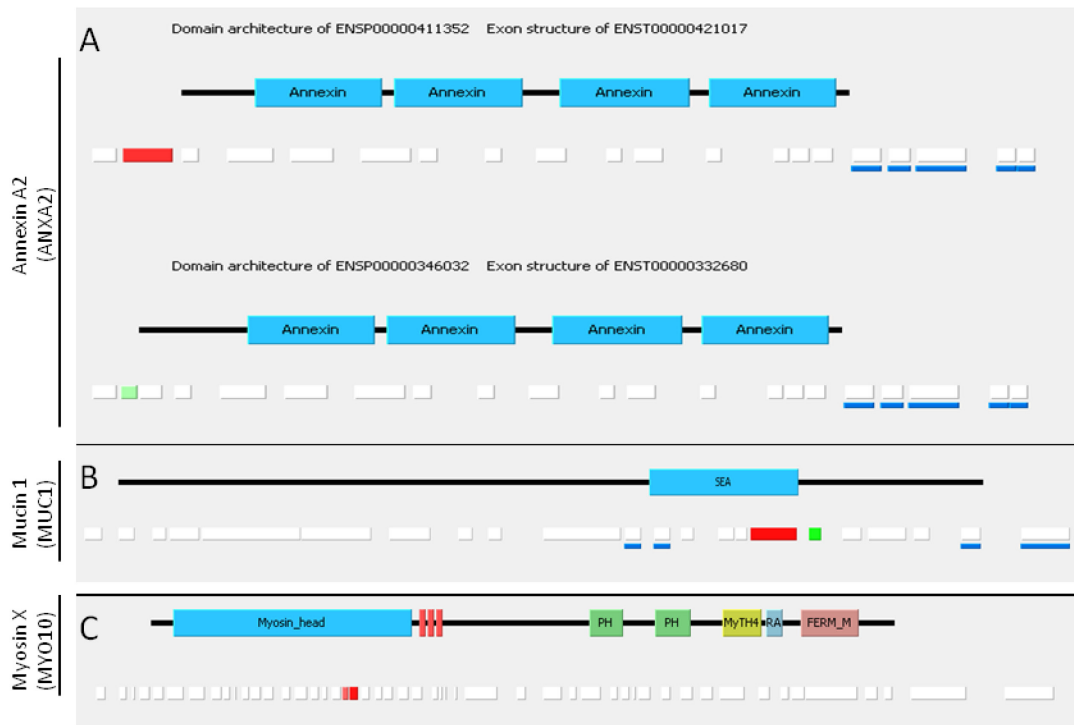
Figure 16. Alternative splicing events in PanIN3s. Splicing events from the differential comparison of PanIN3s and normal duct were imported into Cytoscope and mapped with DomainGraph. Each display shows differentially expressed isoforms of that gene. The top bar is conserved domains and the bottom bar is exons. Exon highlights: red = upregulated in PanIN3s, green = downregulated in PanIN3s. A) Annexin-2; B) Mucin 1; C) Myosin 10.

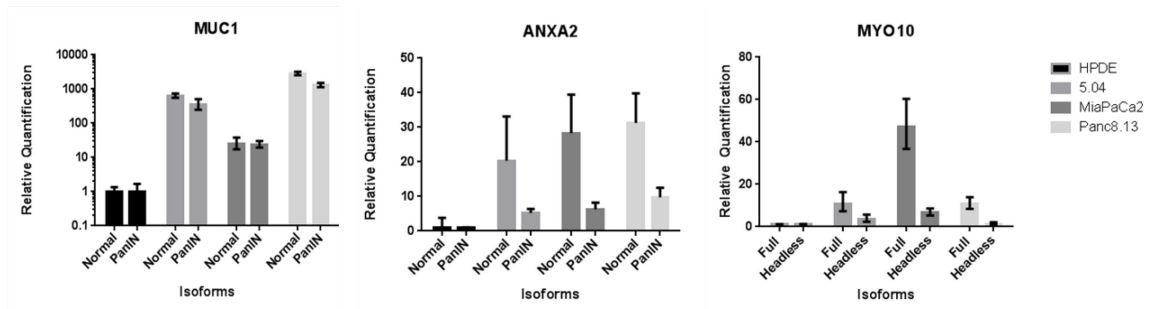**Figure 17. Relative quantification of isoform-specific mRNA in pancreatic cell lines.** One normal pancreatic cell line (HPDE) and 3 cancer cell lines were assayed for specific isoforms of MUC1, ANXA2, and MYO10 by RT-PCR. Relative isoform mRNA levels after normalization to the corresponding 18S rRNA are shown.
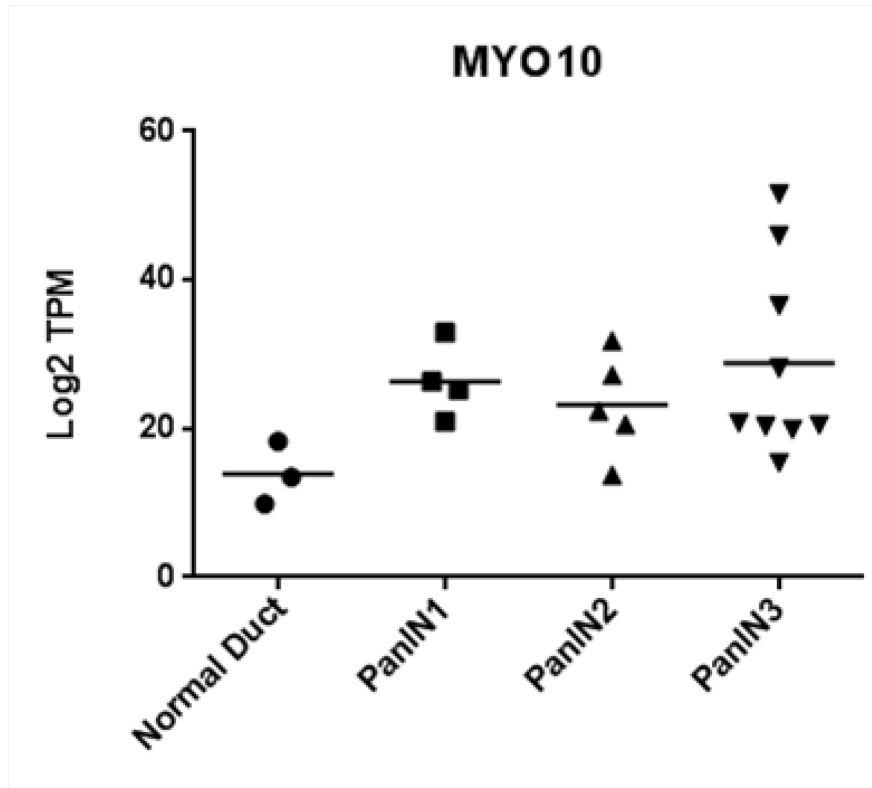
Figure 18. MYO10 mRNA expression. MYO10 is overexpressed 2.07-fold in PanIN3s compared to normal ducts.
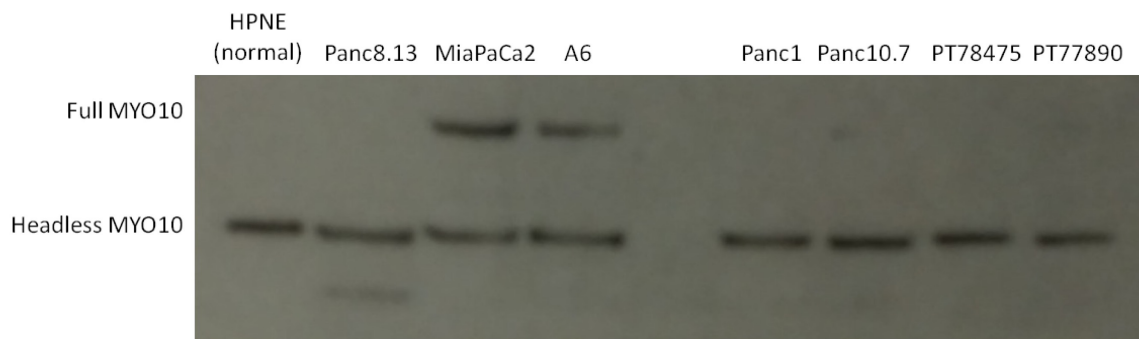
Figure 19. MYO10 protein isoform expression in cell lines and patient samples. All tested samples are positive for the headless isoform. MiaPaCa2 and A6 pancreatic cancer cell lines are positive for the full isoform. HPNE = normal pancreatic cell line; Panc8.13, MiaPaCa2, A6, Panc1, and Panc10.7 = pancreatic cancer lines; PT78475 and PT77890 = primary pancreatic cancer samples.
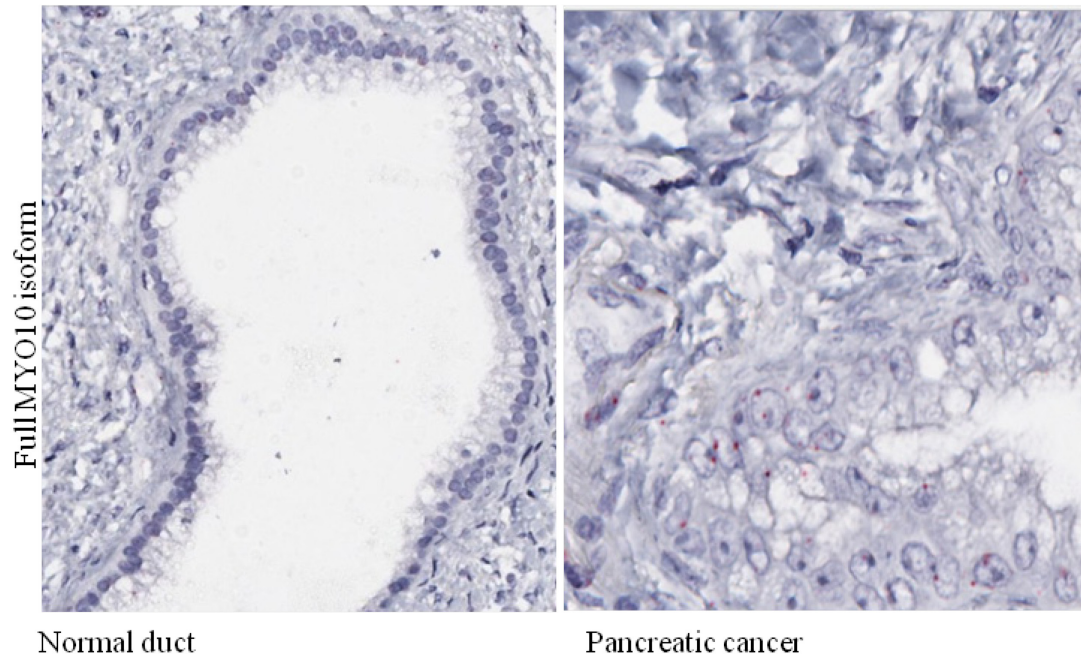
Figure 20. RNA in situ hybridization analysis of full MYO10 isoform expression in pancreatic cancer tissue. TMAs were assayed with an isoform-specific probe for full MYO10 mRNA. Though both normal pancreatic ductal cells and pancreatic cancer cells express this isoform, expression is significantly higher in the latter.

Chapter 3. Susceptibility of ATM-deficient pancreatic cancer cells to DNA-damaging therapies

BACKGROUND

ATM is a phosphatidylinositol 3-kinase-like kinase (PIKK) that has an apical role in orchestrating the complex DNA damage response (DDR)[133], chromatin remodeling, response to oxidative stress[134], and other cellular functions. Germline, biallelic inactivation of *ATM* causes the severe, developmental, neurodegenerative disease Ataxia Telangiectasia[135], which carries a 25% lifetime risk of cancer due to an inability to respond effectively to double-stranded breaks (DSBs) in DNA. Monoallelic inactivating variants of *ATM* and deletion of the wild type allele are observed in a small percentage of familial PDAC cases, implicating ATM as a cancer suppressor subject to the 2-hit model [136]. Exome sequencing data of human PDAC and progenitor lesions has revealed Ataxia Telangiectasia Mutated (ATM) to be one of the 16 most commonly mutated genes in human PDAC[137] and followup immunohistochemical studies have observed ATM protein loss in 38/347 (11%) of sporadic cancers and in 12 out of 49 (24.5%) of familial cancers[138]. Additionally, tumoral loss of ATM was a predictor of decreased overall survival, suggesting ATM loss plays a very active role in cancer progression.

The nature of this role is not yet fully clear. Deletion of ATM in a mouse PDAC model has also been shown to induce epithelial-mesenchymal transition and shorter survival[139]. It is notable that ATM is frequently inactivated by somatic mutation in other cancers and its status is a strong predictor for treatment outcome with DNA-damaging agents, albeit one that can cut both ways. In many cases, loss of ATM sensitizes cancer cells to chemotherapeutics. For example, suppression of ATM in p53 deficient MEFs sensitizes them to doxorubicin [140]. ATM-deficient chronic lymphocytic leukemia cells suffered a synthetic lethal effect when treated with an ATR inhibitor[141]. In glioblastoma cells, ATM expression directly correlated with radioresistance[142]. Conversely, due to its role in triggering cell cycle arrest and apoptosis, ATM inactivation confers resistance to therapy in other cancers[143]. High-mobility group A proteins positively regulate ATM expression, promoting chemoresistance[144]. These paradoxical outcomes are thought to be

related to differences in the effects of ATM inactivation depending on p53 status: p53-deficient cells depend on ATM signaling for survival[145] while ATM inactivation in p53-expressing cells confers chemoresistance[140, 146].

DDR Cascade

DNA damage in cells is conventionally inflicted by ionizing radiation, reaction with free radicals, or enzymatic excision and can take the form of either single stranded breaks (SSBs) or DSBs. DSBs are a dire threat to cells if left unaddressed because they can result in senescence or gross chromosomal rearrangements (GCRs) that give rise to cell death or cancer[147]. Though less threatening and more easily repaired, SSBs can be compounded into DSBs by cell division or by two proximal lesions on opposite strands. Cell division is also when the genome is at its most vulnerable to DNA damage in general and the conversion of DSBs into GCRs. As a result of this and their frequent attenuation of DNA repair pathways, rapidly-dividing cancer cells are especially sensitive to DNA damaging agents.

In healthy cells, ATM exists as a quiescent homodimer activated in an overlapping, multi-stepped process in the presence of DSBs[148]. ATM is recruited to these lesions by the rapid-response damage sensor MRE11-RAD50-NBS1 (MRN) complex, which resects the breakpoint ends, shedding short, single-stranded (ssDNA) oligonucleotides. The exact mechanism and timing of ATM activation is a subject of some ambiguity, but it has been shown that association with these ssDNA oligos with or without MRN recruitment is sufficient and that their absence causes a rapid extinction of ATM activity[149]. Conversely, it has also been shown that prolonged association of ATM with undamaged chromatin in the absence of ssDNA oligonucleotides can also trigger activation[150]. Activation is marked by acetylation of lysine 3016[151] and autophosphorylation at four sites[152], causing a dissociation of the dimer to an active monomer state. These modifications are required for retention of ATM at DSBs, but not its initial

recruitment[153]. Upon recruitment and sustained activation, ATM associates directly with and phosphorylates RAD50 and NBS1[154-157]. These associations are critical to the retention of ATM and signaling of downstream effectors with sweeping effects on the cell.

One of the first of these effects is initiation of one of the major repair mechanisms. The most common of these is classical nonhomologous end joining (C-NHEJ), in which DSBs are rapidly repaired by the downstream ATM targets KU70, KU86, DNA-PKcs, LIG4, XRCC4, XLF and Artemis[147]. If rapid repair is impossible because of complications to the break or a deficiency in the C-NHEJ proteins, resection at the DSB ends occurs, exposing single stranded breaks (SSBs) that engage either homologous recombination repair (HRR) or alternative nonhomologous end joining (A-NHEJ)

Especially important is ATM's role in cell cycle arrest, which allows time to repair damage without compounding it through cellular division. To this end, one of the key proteins phosphorylated by ATM is H2AX, which forms characteristic foci at the site of DSBs. These foci recruit 53BP1 (p53), which both amplifies ATM downstream signaling and can itself be phosphorylated and activated by ATM[158-160]. This activation is enhanced by several other proteins phosphorylated by ATM, including CHK2, STRAP, and HNRNPK. ATM-phosphorylated MDM2 conversely acts as an ubiquitin ligase on p53[161, 162]. Activation of p53 induces transcription of several genes that trigger cell cycle arrest such as p21[163] as do ATM-phosphorylated CHK1 and CHK2[164, 165]. Context-dependent modulation of activated p53 and its downstream signals can alternatively push the cell into senescence, autophagy, or apoptosis if breaks cannot be efficiently repaired.

The overarching scope of ATM's role in the DDR and other pathways has been repeatedly expanded. Proteomic screens have identified over 700 proteins bearing one or more consensus sites for ATM phosphorylation[166]. This scope is perhaps not surprising given the far-

reaching implications that pausing the cell cycle has for routine operations in the cell, and it is thought that ATM activation modulates many aspects cellular metabolism, DNA transcription, and protein synthesis[167, 168].

Redundancy in DDR Pathways

The importance of DNA repair to cells necessitates redundancy in its response, and much of the damage can be repaired even in the absence of ATM. Ataxia telangiectasia and Rad3-related (ATR) is another member of the PIKK kinase family that responds to a broader range of DNA damage than ATM, including stalled replication forks and pyrimidine dimers in addition to DSBs[169]. ATR recruitment and activation is dependent on the association of ATR interacting protein (ATRIP) and replication protein A (RPA) at a single-stranded DNA (ssDNA) locus[170]. RPA-ssDNA is a common intermediate produced by stalled replication forks, resection at DSB ends, and nucleotide excision repair (NER)[171]. Once activated, ATR phosphorylates many of the same targets as ATM regulating repair, cell cycle checkpoints, and apoptosis. Additionally, ATR is capable of stabilizing and restarting stalled replication forks. This property makes ATR indispensable to the survival of proliferating cells.

The DNA-dependent protein kinase (DNA-PK) is another key PIKK player in DNA repair pathways. The catalytic subunit of DNA-PK, DNA-PKcs, responds to DSBs, phosphorylating many of the same targets as ATM and ATR. DNA-PKcs phosphorylates residues of polo-like kinase (PLK1), H2AX, and CHK2 that respond specifically to errors in mitosis. Deletion or inhibition of DNA-PKcs leads to abnormal nuclear morphologies resulting from misaligned mitotic chromosomes during segregation[172]. In lieu of ATM function, both ATR and DNA-PKcs are capable of repairing many of the DSBs that might otherwise prove intolerable to the cell.

ATM-dependent repair

The broad redundancies in DDR signaling are somewhat paradoxical given the severity of the A-T disease. The reason for this is that while the vast majority of DSBs can be repaired by ATM, ATR, or DNA-PKcs somewhat interchangeably, a small subset are truly ATM-dependent. Observing DNA repair kinetics, Riballo *et al.* showed that most DSBs are repaired within 4 hours, but approximately 10% of 'higher complexity' DSBs require up to 24 hours[173]. ATM-deficient cells were exclusively deficient in the latter, and in experiments they were retained as long as 14 days later. Repair of these breaks required both the sustained cell cycle arrest of functional ATM and greater processing of breakpoint ends. More recently, it has been shown that ATM-dependent DSBs occur in areas that are stoichiometrically difficult for repair complexes to access; because they either consist of several DSBs in close proximity or they occur in regions where DNA binding elements and chromatin condensation block out other proteins, such as heterochromatin[174] and telomere-adjacent regions[175]. ATM is capable of inducing chromatin relaxation through histone modifications such as monoubiquitylation of H2B[176] and hyperacetylation of H4[177].

Other experiments of the Riballo *et al.* study showed that radiation, at doses causing the same number of DSBs as etoposide, caused a greater proportion of high complexity, ATM-dependent DSBs[173]. It is possible that the same circumstances that make these breaks difficult for repair proteins to reach are also often inaccessible to chemical agents, but not radiation. A key and characteristic aspect of A-T disease is acute radiosensitivity.

We examine the functional impact of ATM depletion on pancreatic cancer cells. We test ATM-deficient cells for increased sensitivity to a variety of chemotherapeutic agents and radiation. Finally, we examine the effect of radiation on DNA integrity in ATM-deficient PDAC cells.

MATERIALS AND METHODS

<u>shRNA inhibition of ATM</u>

Hairpin shRNA sequences targeting ATM were designed with the Oligoengine software (www.oligoengine.com) and ordered from Integrated DNA Technologies (www.idtdna.com):

Forward : 5'-

AGCTTAAAAAGAGGTCAAACCTAGAAAGCTCTCTTGAAGCTTTCTAGGTTTGACCTC

GGG

Reverse : 5'-

GATCCCCGAGGTCAAACCTAGAAAGCTTCAAGAGAGCTTTCTAGGTTTGACCTCTTTT

TA

Sequences were annealed and ligated into linearized pSuper.retro.puro vector provided by Salvador Suarez Naranjo in the lab of Dr. Christine Iacobuzio-Donahue. Subcloning Efficiency DH5α Competent Cells (ThermoFisher) were transformed with constructs and selected with 100 µg/ml ampicillin LB agar plates. Isolated bacteria were grown overnight in liquid LB broth with 100 µg/ml ampicillin and processed for plasmid using a GeneJET Plasmid Miniprep Kit (ThermoFisher). Harvested plasmid was checked for correct insertion by Sanger sequencing (5'-GGAAGCCTTGGCTTTTG).

1.5 µg of pSuper construct and 1 µg of amphotropic envelope expression vector (pVSV-G) were used to transfect GP-293 cells (ATCC) in 6-well dishes using Lipofectamine 2000 (Life Technologies) according to the manufacturer's protocol. Medium was changed after 24 hours. After an additional 24 hours, cell culture supernatants were harvested, filtered with 0.22 µm filters, and diluted 1:2 in fresh medium. Polybrene was added to diluted viral supernatant at 6 ug/mL which was then added to cells at 30% confluency in 6-well plates. After 24 hours, viral

media was replaced with fresh media. After an additional 48 hours, media was replaced with fresh media containing Puromycin Selection continued for 7 days.

Western Blot

Total protein lysates were extracted in RIPA buffer (Roche Diagnostics, Indianapolis, IN) with cOmplete Mini tablets (Roche Diagnostics) and homogenized with a Bioruptor (Diagenode, Denville, NJ) for 8 cycles (30s high, 30S off).   Protein concentrations were determined using the Pierce BCA Protein Assay Kit (ThermoScientific, Waltham, MA). Membranes were incubated overnight at 4º C with primary antibodies: rabbit anti-ATM (Abcam, Cambridge, MA) or goat anti-Actin (Santa Cruz Biotechnology). Membranes were incubated with horseradish peroxidase (HRP)-conjugated secondary antibody in 5% dry milk for 1 hour. Bound antibody was detected with a Pierce ECL Plus kit (ThermoScientific).

Chemosensitivity

Chemosensitivity assays were performed using a protocol previously described[178]. In brief, cells were plated at a density of 3,000 cells/well in the 60 center wells of 96-well plates. Edge wells were filled with PBS. Media was aspirated 24 hours later and replaced with 200 ul/well drug-supplemented media. Drugs were serially diluted 10-fold in standard growth medium at concentrations ranging from 1 nm to 100 um. For drugs dissolved in dimethyl sulfoxide (DMSO) vehicle, untreated cells were incubated in DMSO-supplemented media as a negative control. Plates were incubated for 72 hours. 10% AlamarBlue Cell Viability reagent (ThermoFisher Scientific) was added to each well as per the manufacturer's protocol.   Readings were performed using a BMG FluoStar Galaxy instrument (BMG LAbtechnologies; excitation at 544 nm, reading at 590 nm). Statistical analyses were performed and ic50 curves were generated using Graphpad Prism 6.0.

Radioclonogenicity

We utilized a protocol described by Dr. James Eshleman. Cells were plated at low density (9 cells/well Panc2.5 and MiaPaCa2, 45 cells/well Panc8.13) and irradiated in a Gammacell 40A (cesium-137 source) at 0/2/4/6 Gy, then allowed to grow until distinct colonies of >50 cells were countable in untreated plates (8-21 days, depending on cell line). For fractionated radiation experiments, doses were delivered every 24 hours. Staining was performed with Crystal Violet solution (5% Crystal Violet, 25% methanol) and wells with 1 or more colonies of >50 cells were counted. Cloning efficiency was calculated as: (-ln(total wells-clone wells/total wells))/(number of cells/well) normalized to the number of clone-positive wells on untreated plates.

Chemoradioclonogenicity

Cells were plated at low density (9 cells/well) and allowed to attach overnight. Media was replaced by serially-diluted drugs at 16 wells/dose: MiaPaCa2 (1 nm-10 μm Ve821 ATR inhibitor) and Panc2.5 (1 nm-1 μm Nu7441 DNA-PKcs inhibitor). Plates were irradiated in a Gammacell 40A at 0/1/2/4/6 Gy (MiaPaca2) and 0/2/4 Gy (Panc2.5). After 14 days, staining was performed with Crystal Violet solution and wells with 1 or more colonies of >50 cells were counted. Cloning efficiency was calculated as previously.

Comet Assay

Comet assay was performed with a protocol provided by Dr. Mohammad Hedeyati. Cells were detached and resuspended in 5 ml media at 2×10^5 cells/ml stored on ice to minimize DNA damage from handling. CometAssay LMAgarose (Trevigen, Gaithersburg, MD) was kept ready in a 37º water bath. On ice, cells were irradiated in a Gammacell 40A at 4 Gy.

50 μl of cells were combined with 400 μl of LMAgarose and gently mixed. 50 μl of mix was added to each well of a Flare Slide (Trevigen) and spread evenly with a pipet tip. Slides were immediately incubated on a 4º metal surface to cool. Chilled slides were immersed in a

glass dish filled with CometAssay Lysis Solution (Trevigen) for 1 hour at 4º C. Slides were washed twice for 15 min in TBE solution and electrophoresed for 40 minutes at 4º C in TBE buffer using 1 V/cm length of the box. DNA was stained with DAPI ProLong Gold Antifade Mountant (ThermoFisher Scientific) and imaged on a Confocal Eclipse Ti-E microscope (Nikon Instruments, San Quirico, Italy). Pictures were taken of 100 cells for each sample and analyzed with CometAssay software (www.autocomet.com).

RESULTS

Inhibition of ATM

In order to understand the role played by ATM in pancreatic cancer cells, we knocked down expression of ATM in two cell lines expressing mutant p53 (MiaPaCa-2, Panc2.5) and one cell line expressing wild type p53 (Panc8.13) using shRNA constructs targeting ATM. (Figure 1).

Chemosensitivity

We treated our ATM-deficient cells with serial dilutions of a variety of chemotherapeutic agents and measured their viability. We focused primarily on DNA-damaging agents, including gemcitabine, olaparib, cisplatin, topotecan, doxorubicin, and mitomycin c. We also examined agents inhibiting other DNA repair factors in the hopes of exploiting synthetic lethality including Ve821 (ATR inhibitor) and Nu7441 (DNA-Pkcs inhibitor).

Although most of these agents inflicted substantial mortality on all of the tested lines, we observed no difference in the chemosensitivity of ATM-deficient cells vs. ATM wild type cells (Figure 2). We conclude that ATM-deficient pancreatic cancer cells do not have increased sensitivity to any of the agents tested.

Radioclonogenicity

It has long been known that patients with ATM are exceptionally sensitive to DNA damage induced by radiation. Although ATM deficiency might be expected to induce radiosenstivity in pancreatic cancer cells, pancreatic cancer is a relatively radioresistant cancer and it is known if ATM deficiency would render pancreatic cancer cells radiosensitive. We sought to determine if our ATM-deficient PDAC cells exhibited this effect by calculating the cloning efficiency of irradiated cells. Panc2.5, MiaPaCa-2, and Panc8.13 lines showed markedly reduced cloning efficiency at all radiation doses in ATM-deficient cells compared to ATM wild type cells (Figure 3). In all three lines, the difference in cloning efficiency between ATM-deficient and wild type cells grew with each radiation dose. While surviving wild type clones generally appeared healthy and stable at lower doses, surviving ATM-deficient cells at any dose frequently exhibited aberrations: cell enlargement, multinucleation, and twisted, malformed cell boundaries. Such changes are known to be markers of cells enduring sustained genotoxic insult[179].

It is possible that many ATM-deficient cells were able to survive irradiation by repairing DSBs with compensatory DNA repair mechanisms such as ATR and DNA-PKcs. We repeated our radioclonogenicity assays on MiaPaCa2 with simultaneous application of an ATR inhibitor and on Panc2.5 with a DNA-PKcs inhibitor. In each case, we saw no multiplicative impact on cloning efficiency of ATM-deficient cells that would suggest a synergistic interaction of the agents (Figure 4).

Another strategy to improve radiosensitivity of cancer cells is to fractionate large doses of radiation into several smaller doses. The sensitivity of DNA to radiation damage varies across the cell cycle, with greater vulnerability during G2 and M phases and greater resistance during the S phase[180]. By delivering multiple doses of radiation at different timepoints, different fractions of rapidly-dividing cancer cells may be caught during their more sensitive phases. Additionally, hypoxic cells within the mass of the cancer are known to have increased resistance to radiation.

As peripheral, sensitive cells are killed by early doses, oxygen is able to reach internal cells, sensitizing them in turn to successive doses. Fractionated radiation is also appealing because it is less toxic for the patient than a single, high dose. The lower amounts of DNA damage inflicted by lighter exposures can be tolerated and repaired by normal cells in-between doses. Cancer cells that have their DNA repair mechanisms attenuated may be unable to repair even small amounts of damage efficiently, allowing repeated doses to have a compounding effect that results in halted replication and apoptosis.

We applied fractionated radiation doses to ATM-inhibited Panc2.5 and Panc8.13 cells. Cells were treated with either 5 Gy or a therapeutically equivalent 6 Gy over 3 doses of 2 Gy each. We find that in both lines, the fractionated doses were marginally more effective at inhibiting clonogenic growth than the single 5 Gy dose against ATM-deficient, but not ATM wild type cells (Figure 23).

We were additionally interested in whether any synergistic effect could be observed between treatment with olaparib, a PARP inhibitor, and fractionated radiation. We repeated our fractionated radioclonogenicity assay on Panc2.5 and Panc8.13 cells, treating cells with 100 nm Olaparaib 1 hour before each radiation dose. In both cell lines, we observed total loss of clonogenicity in ATM-inhibited cells that were treated with olaparib or DMSO (control) and 3 doses of 2 Gy radiation. We additionally observed a total loss of clonogenicity in Panc8.13 ATM wild type cells treated with olaparib and 3 doses of 2 Gy radiation.

DNA Damage

Several assays exist to assess DNA damage by imaging and quantifying foci of response factors such as H2AX, but given ATM's apical role in recruiting many of these factors to DSBs, we resolved to examine the DNA of cells directly. In the comet assay, treated cells are embedded in slide-mounted agarose and lysed to form nucleoids of entangled, supercoiled DNA.

Electrophoresis of the nucleoids results in a 'tail' of broken DNA fragments extruding that resembles a comet. By staining the DNA and measuring the proportional intensity of radiation in the head and tail of the comet, we can determine the extent of DNA damage that has occurred.

Treating MiaPaCa-2 cells with 4 Gy radiation, we observe a reduced fraction of DNA in the comet head of cells immediately post-exposure (Figure 25A). This loss was equal between wild type and ATM-deficient cells, reflecting no difference in the amount of DNA damage inflicted. This was unsurprising as ATM should not affect the rate at which DNA damage occurs in the cell, but rather its ability to tolerate and repair that damage.

With that in mind, we next used the comet assay to quantify the repair kinetics of MiaPaCa-2, Panc2.5, and Panc8.13 cells in the hours post-exposure to 4 Gy radiation. In all three lines, we observed comparable DNA damage in wild type and ATM-deficient cells immediately post-exposure. This was followed by a small but significant difference in the amount of DNA repaired at later timepoints between wild type and ATM-deficient cells: Panc8.13, 11% at 14 hours (p-value = 1.45732×10^{-11}) (Figure 25B); MiaPaCa-2, 14% at 24 hours (p-value = 0.00006) (Figure 25C); Panc2.5, 8% at 48 hours (p-value = 0.00006) (Figure 25D). This result is highly consistent with past findings that the repair of 10-15% of DSBs is ATM-dependent[173].

DISCUSSION

Much recent attention in cancer has been devoted to the concept of targeted therapy: a strategy of matching treatments to the specific genetic landscape of a patient's disease. Because pancreatic cancer has proven particularly resistant to non-surgical interventions, identification of markers for cancers excepted from this rule would be very valuable. Next generation sequencing (NGS) is enabling the detection of mutations in pancreatic cancers in the clinic. And in a recent study, an ATM mutation was detectable by targeted NGS in endoscopic ultrasound fine needle aspirate cytology samples[181].

Interestingly, we were unable to identify differential chemosensitivity of pancreatic cancer cells with ATM-deficient cells compared to parental cells with intact ATM. This was the case for the Parp inhibitor, olaparib: in vitro studies [182] and clinical trials have found PARP inhibitors such as olaparib to be especially effective in ATM-deficient breast and prostate cancers[183, 184].

In all three lines tested, ATM-deficient PDAC showed a marked loss of ability to form proliferative colonies post-irradiation in comparison to PDAC cells expressing wild type ATM.We also assayed DNA repair kinetics for irradiated cells. We determined that in ATM-deficient PDAC cells, ~10% more DSBs are retained at 48 hours than in ATM wild type cells. Our study supports the hypothesis that ATM-deficient pancreatic cancers are radiosensitive. Our results provide the rationale for testing this hypothesis in a clinical trial.
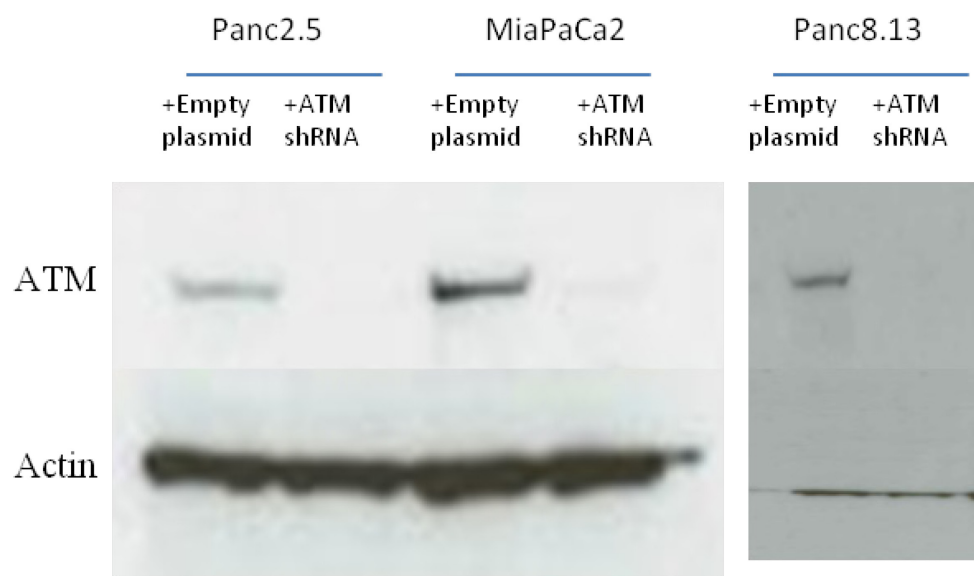
Figure 21. shRNA-mediated knockdown of ATM.

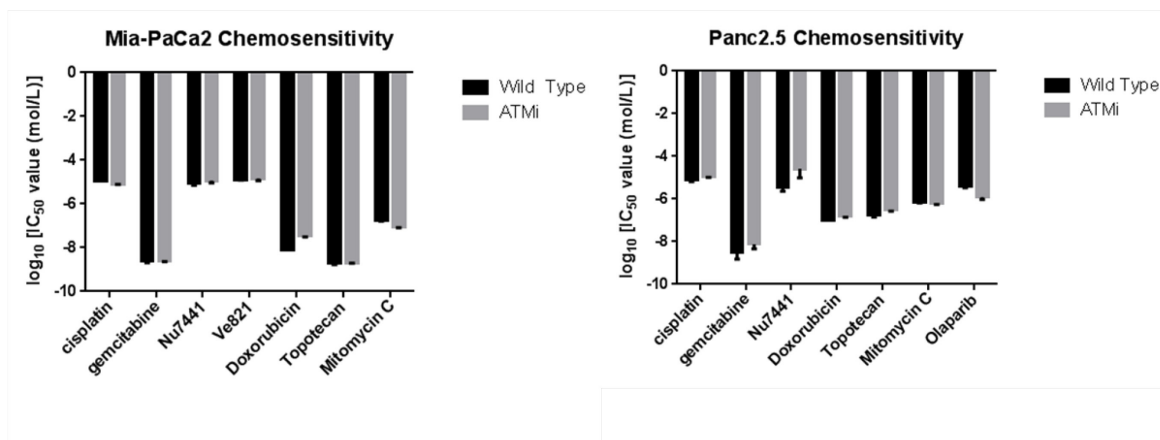**Figure 22. Chemosensitivity of ATM-deficient pancreatic cancer cell lines**. Cells were exposed to serial dilutions of each agent from 1 nm to 100 um for three days, then assayed for viability with AlamarBlue. Ic50 values were calculated from the dose-response curve. Mia-PaCa2 and Panc2.5 cells deficient in ATM did not show any increased sensitivity to chemotherapeutic agents tested in comparison to wild type cells.
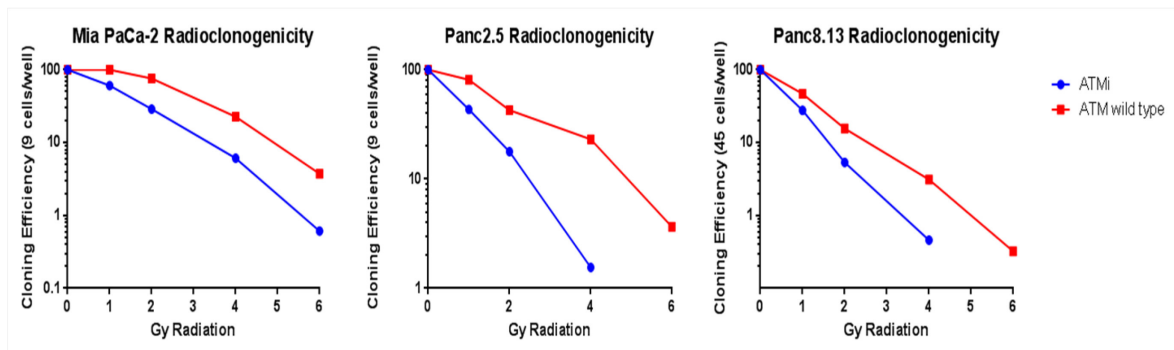
Figure 23. Radiosensitivity of ATM-deficient pancreatic cancer cell lines. Cells were plated at 96 wells and irradiated. After 14-21 days, positive wells were counted as those with one or more colonies of >50 cells, cloning efficiencies were calculated for each condition, and normalized to the untreated cells of each cell line. In all three lines tested, ATM inhibition resulted in marked radiosensitivity in comparison to wild type cells.
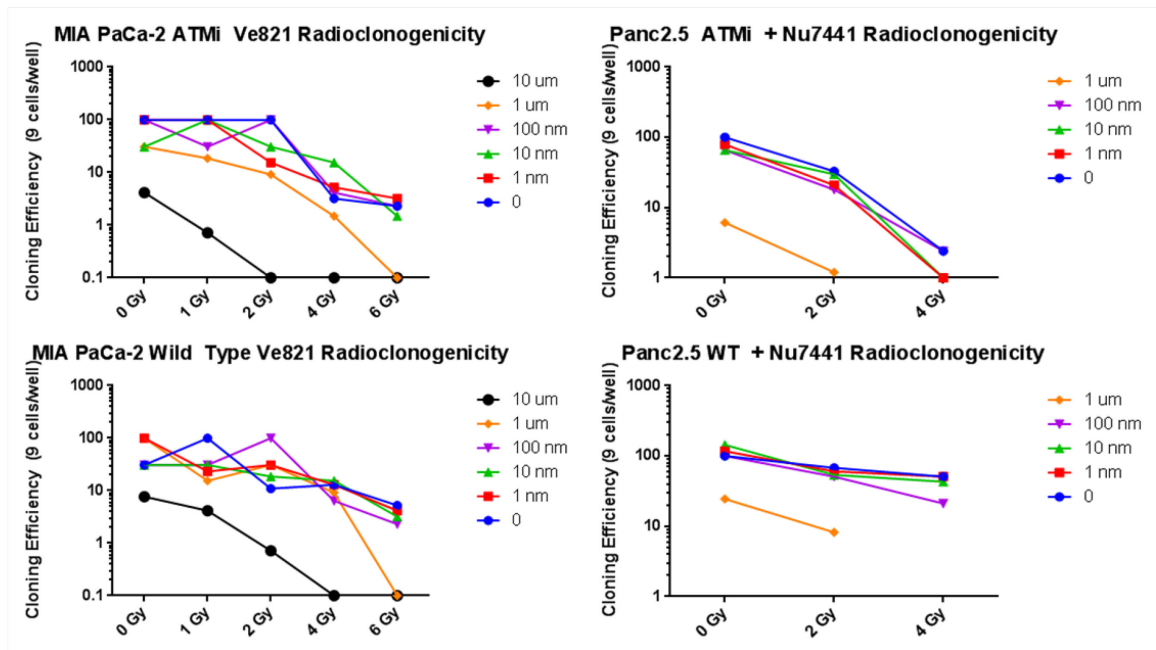
Figure 24. Chemoradioclonogenicity of ATM-deficient cells. Cells were plated at 96 wells and treated with Ve821 ATR inhibitor (MIA PaCa-2 cells, A, B) or Nu7441 DNA-PKcs inhibitor (Panc2.5 cells, C, D) one hour before irradiation. After 14-21 days, positive wells were counted as those with one or more colonies of >50 cells, cloning efficiencies were calculated for each condition, and normalized to the untreated cells of each cell line. There was no synergistic effect between inhibition of ATR or DNA-PKcs and radiosensitivity at low doses of the drug.
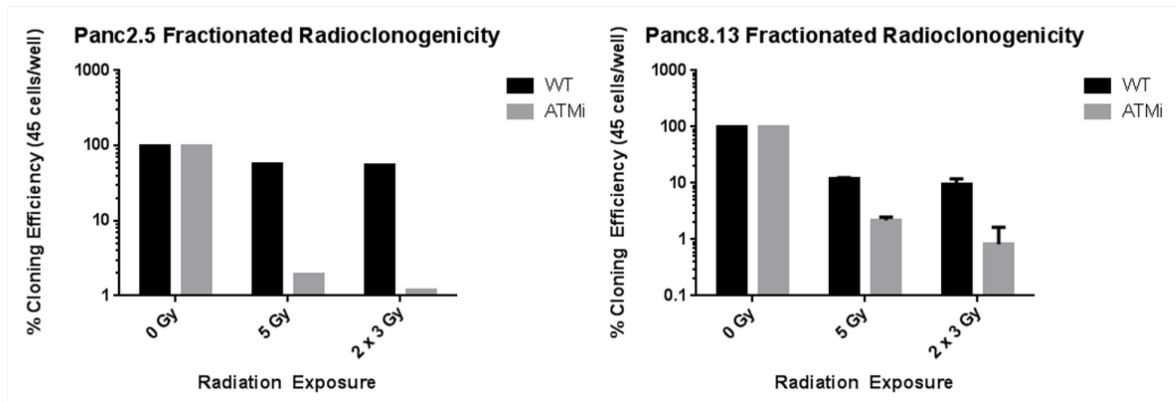
Figure 25. Cells were plated on 96-well plates and irradiated. Fractionated radiotherapy doses were applied every 24 hours. CE values were calculated from the number of wells out of 96 containing clones of 50 or more cells for each treatment. CE values were normalized to the CE values of each untreated cell line. ATM-deficient cells in both cell lines were slightly more sensitive to fractionated radiotherapy than single dose radiotherapy.
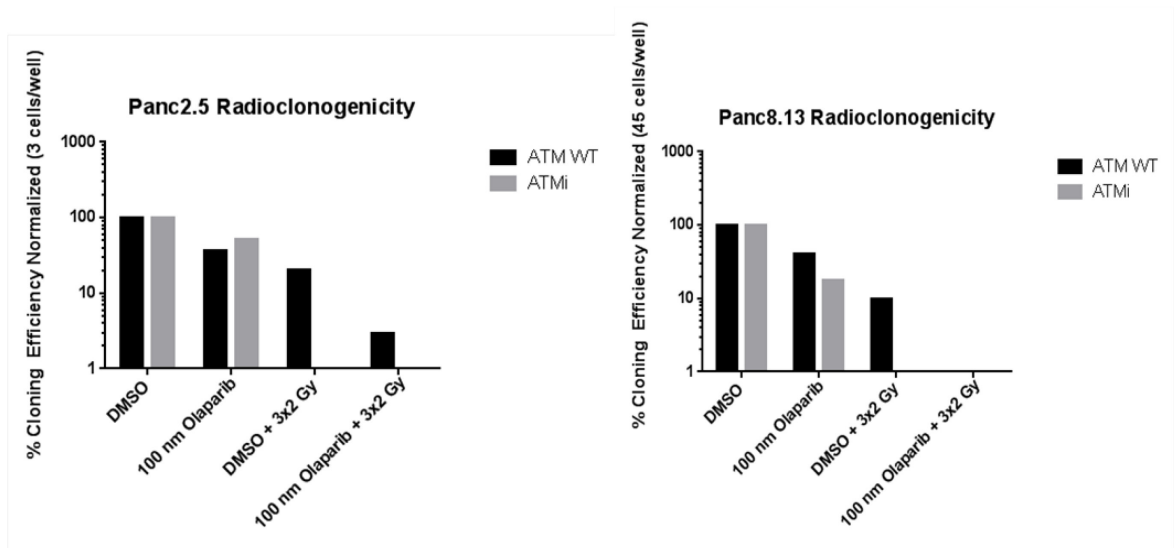
Figure 26. Combination therapy of Olaparaib and fractionated radiation. Cells were plated on 96-well plates. Every 24 hours, media was replaced with normal media + 100 nm Olaparib or normal media + 0.1% DMSO. Fractionated radiotherapy doses were applied one hour after changing media. CE values were calculated from the number of wells out of 96 containing clones of 50 or more cells for each treatment. CE values were normalized to the CE values of each untreated cell line. ATM-deficient cells in both cell lines were slightly more sensitive to fractionated radiotherapy than single dose radiotherapy.
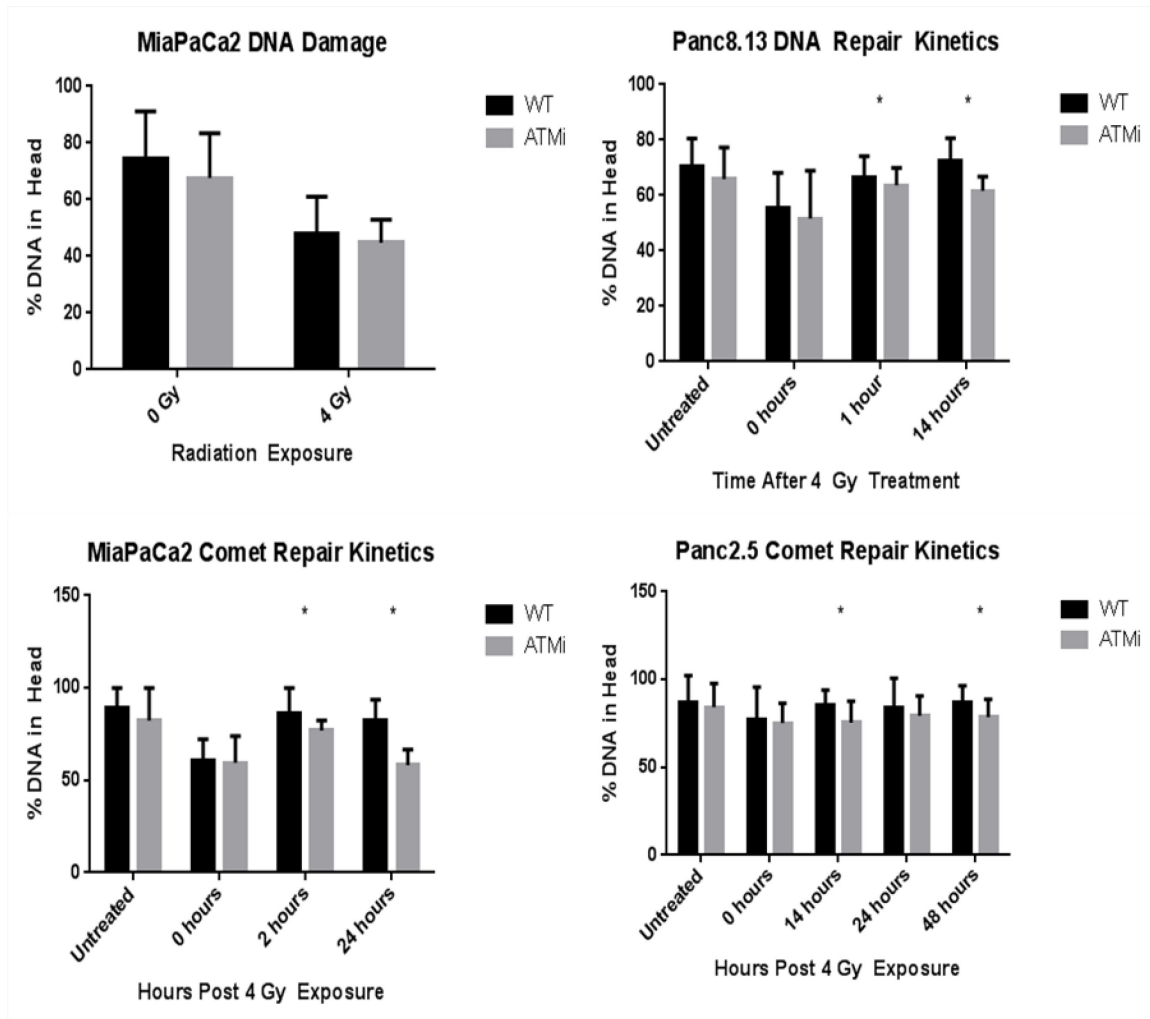
Figure 27. DNA repair kinetics of ATM-deficient cells. The comet assay was used to evaluate DNA damage in cells post-irradiation. For each condition, 100 cells were imaged and analyzed for the proportion of DNA in their head (intact) and tail (damaged). A) Immediately post-irradiation, there is no significant difference in the proportion of damaged DNA between ATM-deficient and wild type cells. B-D) The comet assay was performed on cells at multiple timepoints post-irradiation. In all three cell types, the percentage of DNA in comet heads was significantly lower in ATM-deficient cells in comparison to wild type cells.

REFERENCES

1. Siegel, R.L., Miller, K.D. & Jemal, A. Cancer statistics, 2016. *CA Cancer J Clin* **66**, 7-30 (2016).
2. Wolfgang, C.L. et al. Recent progress in pancreatic cancer. *CA Cancer J Clin* **63**, 318-48 (2013).
3. Katz, M.H. et al. Long-term survival after multidisciplinary management of resected pancreatic adenocarcinoma. *Ann Surg Oncol* **16**, 836-47 (2009).
4. Verbeke, C.S. & Gladhaug, I.P. Resection margin involvement and tumour origin in pancreatic head cancer. *Br J Surg* **99**, 1036-49 (2012).
5. Thorban, S., Roder, J.D. & Siewert, J.R. Detection of micrometastasis in bone marrow of pancreatic cancer patients. *Ann Oncol* **10 Suppl 4**, 111-3 (1999).
6. Winter, J.M. et al. 1423 pancreaticoduodenectomies for pancreatic cancer: A single-institution experience. *J Gastrointest Surg* **10**, 1199-210; discussion 1210-1 (2006).
7. Herman, J.M. et al. Analysis of fluorouracil-based adjuvant chemotherapy and radiation after pancreaticoduodenectomy for ductal adenocarcinoma of the pancreas: results of a large, prospectively collected database at the Johns Hopkins Hospital. *J Clin Oncol* **26**, 3503-10 (2008).
8. Conroy, T. et al. FOLFIRINOX versus gemcitabine for metastatic pancreatic cancer. *N Engl J Med* **364**, 1817-25 (2011).
9. Gnerlich, J.L. et al. Microscopic margins and patterns of treatment failure in resected pancreatic adenocarcinoma. *Arch Surg* **147**, 753-60 (2012).
10. Chatterjee, D. et al. Histologic grading of the extent of residual carcinoma following neoadjuvant chemoradiation in pancreatic ductal adenocarcinoma: a predictor for patient outcome. *Cancer* **118**, 3182-90 (2012).
11. Neoptolemos, J.P. et al. A randomized trial of chemoradiotherapy and chemotherapy after resection of pancreatic cancer. *N Engl J Med* **350**, 1200-10 (2004).
12. Hezel, A.F., Kimmelman, A.C., Stanger, B.Z., Bardeesy, N. & Depinho, R.A. Genetics and biology of pancreatic ductal adenocarcinoma. *Genes Dev* **20**, 1218-49 (2006).
13. Almoguera, C. et al. Most human carcinomas of the exocrine pancreas contain mutant c-K-ras genes. *Cell* **53**, 549-54 (1988).
14. Caldas, C. et al. Frequent somatic mutations and homozygous deletions of the p16 (MTS1) gene in pancreatic adenocarcinoma. *Nat Genet* **8**, 27-32 (1994).
15. Redston, M.S. et al. p53 mutations in pancreatic carcinoma and evidence of common involvement of homocopolymer tracts in DNA microdeletions. *Cancer Res* **54**, 3025-33 (1994).
16. Hahn, S.A. et al. DPC4, a candidate tumor suppressor gene at human chromosome 18q21.1. *Science* **271**, 350-3 (1996).
17. Jones, S. et al. Core signaling pathways in human pancreatic cancers revealed by global genomic analyses. *Science* **321**, 1801-6 (2008).
18. Hruban, R.H., Maitra, A., Kern, S.E. & Goggins, M. Precursors to pancreatic cancer. *Gastroenterol Clin North Am* **36**, 831-49, vi (2007).

19. Terhune, P.G., Phifer, D.M., Tosteson, T.D. & Longnecker, D.S. K-ras mutation in focal proliferative lesions of human pancreas. *Cancer Epidemiol Biomarkers Prev* **7**, 515-21 (1998).

20. Risch, H.A. et al. Population BRCA1 and BRCA2 mutation frequencies and cancer penetrances: a kin-cohort study in Ontario, Canada. *J Natl Cancer Inst* **98**, 1694-706 (2006).

21. Vasen, H.F. et al. Risk of developing pancreatic cancer in families with familial atypical multiple mole melanoma associated with a specific 19 deletion of p16 (p16-Leiden). *Int J Cancer* **87**, 809-11 (2000).

22. Thompson, D. et al. Cancer risks and mortality in heterozygous ATM mutation carriers. *J Natl Cancer Inst* **97**, 813-22 (2005).

23. Lim, W. et al. Relative frequency and morphology of cancers in STK11 mutation carriers. *Gastroenterology* **126**, 1788-94 (2004).

24. Rebours, V. et al. Risk of pancreatic adenocarcinoma in patients with hereditary pancreatitis: a national exhaustive series. *Am J Gastroenterol* **103**, 111-9 (2008).

25. Jones, S. et al. Exomic sequencing identifies PALB2 as a pancreatic cancer susceptibility gene. *Science* **324**, 217 (2009).

26. Lowenfels, A.B. et al. Pancreatitis and the risk of pancreatic cancer. International Pancreatitis Study Group. *N Engl J Med* **328**, 1433-7 (1993).

27. Keiles, S. & Kammesheidt, A. Identification of CFTR, PRSS1, and SPINK1 mutations in 381 patients with pancreatitis. *Pancreas* **33**, 221-7 (2006).

28. Morris, J.P.I.V., Cano, D.A., Sekine, S., Wang, S.C. & Hebrok, M. β-catenin blocks Kras-dependent reprogramming of acini into pancreatic cancer precursor lesions in mice. *The Journal of Clinical Investigation* **120**, 508-520.

29. Guerra, C. et al. Pancreatitis-induced inflammation contributes to pancreatic cancer by inhibiting oncogene-induced senescence. *Cancer Cell* **19**, 728-39 (2011).

30. Childs, E.J. et al. Common variation at 2p13.3, 3q29, 7p13 and 17q25.1 associated with susceptibility to pancreatic cancer. *Nat Genet* **47**, 911-6 (2015).

31. Amundadottir, L. et al. Genome-wide association study identifies variants in the ABO locus associated with susceptibility to pancreatic cancer. *Nat Genet* **41**, 986-90 (2009).

32. Dobbins, M., Decorby, K. & Choi, B.C. The Association between Obesity and Cancer Risk: A Meta-Analysis of Observational Studies from 1985 to 2011. *ISRN Prev Med* **2013**, 680536 (2013).

33. Li, D. & Abbruzzese, J.L. New strategies in pancreatic cancer: emerging epidemiologic and therapeutic concepts. *Clin Cancer Res* **16**, 4313-8 (2010).

34. Bell, E.T. Carcinoma of the pancreas. I. A clinical and pathologic study of 609 necropsied cases. II. The relation of carcinoma of the pancreas to diabetes mellitus. *Am J Pathol* **33**, 499-523 (1957).

35. Pannala, R., Basu, A., Petersen, G.M. & Chari, S.T. New-onset diabetes: a potential clue to the early diagnosis of pancreatic cancer. *Lancet Oncol* **10**, 88-95 (2009).

36. Clark, C.G. & Mitchell, P.E. Diabetes mellitus and primary carcinoma of the pancreas. *Br Med J* **2**, 1259-62 (1961).

37. Bonelli, L. et al. Exocrine pancreatic cancer, cigarette smoking, and diabetes mellitus: a case-control study in northern Italy. *Pancreas* **27**, 143-9 (2003).

38. Maisonneuve, P. et al. Cigarette smoking accelerates progression of alcoholic chronic pancreatitis. *Gut* **54**, 510-4 (2005).

39.   Lowenfels, A.B., Maisonneuve, P., Whitcomb, D.C., Lerch, M.M. & DiMagno, E.P. Cigarette smoking as a risk factor for pancreatic cancer in patients with hereditary pancreatitis. *Jama* **286**, 169-70. (2001).

40.   Blackford, A. et al. Genetic mutations associated with cigarette smoking in pancreatic cancer. *Cancer Res* **69**, 3681-8 (2009).

41.   Wilentz, R.E. et al. Loss of expression of Dpc4 in pancreatic intraepithelial neoplasia: evidence that DPC4 inactivation occurs late in neoplastic progression. *Cancer Res* **60**, 2002-6 (2000).

42.   Hruban, R.H., Goggins, M., Parsons, J. & Kern, S.E. Progression model for pancreatic cancer. *Clin Cancer Res* **6**, 2969-72 (2000).

43.   Hruban, R.H. et al. An illustrated consensus on the classification of pancreatic intraepithelial neoplasia and intraductal papillary mucinous neoplasms. *Am J Surg Pathol* **28**, 977-87 (2004).

44.   van Heek, N.T. et al. Telomere shortening is nearly universal in pancreatic intraepithelial neoplasia. *Am J Pathol* **161**, 1541-7. (2002).

45.   Kanda, M. et al. Presence of somatic mutations in most early-stage pancreatic intraepithelial neoplasia. *Gastroenterology* **142**, 730-733 e9 (2012).

46.   Brosens, L.A., Hackeng, W.M., Offerhaus, G.J., Hruban, R.H. & Wood, L.D. Pancreatic adenocarcinoma pathology: changing "landscape". *J Gastrointest Oncol* **6**, 358-74 (2015).

47.   Schutte, M. et al. Abrogation of the Rb/p16 tumor-suppressive pathway in virtually all pancreatic carcinomas. *Cancer Res* **57**, 3126-30 (1997).

48.   Rosty, C. et al. p16 Inactivation in pancreatic intraepithelial neoplasias (PanINs) arising in patients with chronic pancreatitis. *Am J Surg Pathol* **27**, 1495-501 (2003).

49.   Kanda, M. et al. Mutant TP53 in duodenal samples of pancreatic juice from patients with pancreatic cancer or high-grade dysplasia. *Clin Gastroenterol Hepatol* **11**, 719-30 e5 (2013).

50.   Sato, N., Fukushima, N., Hruban, R.H. & Goggins, M. CpG island methylation profile of pancreatic intraepithelial neoplasia. *Mod Pathol* **21**, 238-44 (2008).

51.   Murphy, S.J. et al. Genetic alterations associated with progression from pancreatic intraepithelial neoplasia to invasive pancreatic tumor. *Gastroenterology* **145**, 1098-1109 e1 (2013).

52.   Hustinx, S.R. et al. Differentially expressed genes in pancreatic ductal adenocarcinomas identified through serial analysis of gene expression. *Cancer Biol Ther* **3**, 1254-61 (2004).

53.   Iacobuzio-Donahue, C.A. et al. Highly expressed genes in pancreatic ductal adenocarcinomas: a comprehensive characterization and comparison of the transcription profiles obtained from three major technologies. *Cancer Res* **63**, 8614-22 (2003).

54.   Argani, P. et al. Mesothelin is overexpressed in the vast majority of ductal adenocarcinomas of the pancreas: identification of a new pancreatic cancer marker by serial analysis of gene expression (SAGE). *Clin Cancer Res* **7**, 3862-8 (2001).

55.   Hassan, R. & Ho, M. Mesothelin targeted cancer immunotherapy. *Eur J Cancer* **44**, 46-53 (2008).

56.   Koopmann, J. et al. Evaluation of osteopontin as biomarker for pancreatic adenocarcinoma. *Cancer Epidemiol Biomarkers Prev* **13**, 487-91 (2004).

57.   Koopmann, J. et al. Serum macrophage inhibitory cytokine 1 as a marker of pancreatic and other periampullary cancers. *Clin Cancer Res* **10**, 2386-92 (2004).

58. Rachagani, S. et al. Mucin (Muc) expression during pancreatic cancer progression in spontaneous mouse model: potential implications for diagnosis and therapy. *J Hematol Oncol* **5**, 68 (2012).

59. Li, A. et al. Pancreatic cancers epigenetically silence SIP1 and hypomethylate and overexpress miR-200a/200b in association with elevated circulating miR-200a and miR-200b levels. *Cancer Res* **70**, 5226-37. Epub 2010 Jun 15. (2010).

60. Li, A. et al. MicroRNA array analysis finds elevated serum miR-1290 accurately distinguishes patients with low-stage pancreatic cancer from healthy and disease controls. *Clin Cancer Res* **19**, 3600-10 (2013).

61. Sato, N. et al. Epigenetic inactivation of TFPI-2 as a common mechanism associated with growth and invasion of pancreatic ductal adenocarcinoma. *Oncogene* **24**, 850-8 (2005).

62. Sato, N., Fukushima, N., Chang, R., Matsubayashi, H. & Goggins, M. Differential and epigenetic gene expression profiling identifies frequent disruption of the RELN pathway in pancreatic cancers. *Gastroenterology* **130**, 548-65 (2006).

63. Vincent, A. et al. Epigenetic silencing of EYA2 in pancreatic adenocarcinomas promotes tumor growth. *Oncotarget* **5**, 2575-87 (2014).

64. Li, A. et al. Pancreatic cancers epigenetically silence SIP1 and hypomethylate and overexpress miR-200a/200b in association with elevated circulating miR-200a and miR-200b levels. *Cancer Res* **70**, 5226-37 (2010).

65. Prasad, N.B. et al. Gene expression profiles in pancreatic intraepithelial neoplasia reflect the effects of Hedgehog signaling on pancreatic ductal epithelial cells. *Cancer Res* **65**, 1619-26. (2005).

66. Segara, D. et al. Expression of HOXB2, a retinoic acid signaling target in pancreatic cancer and pancreatic intraepithelial neoplasia. *Clin Cancer Res* **11**, 3587-96 (2005).

67. Ryu, J.K. et al. Aberrant MicroRNA-155 expression is an early event in the multistep progression of pancreatic adenocarcinoma. *Pancreatology* **10**, 66-73 (2010).

68. Krosting J, L.G. RNase activity in mouse tissue: classification, hierarchy, and methods for control. *Ambion TechNotes* **12** (2005).

69. Li, B., Ruotti, V., Stewart, R.M., Thomson, J.A. & Dewey, C.N. RNA-Seq gene expression estimation with read mapping uncertainty. *Bioinformatics* **26**, 493-500 (2010).

70. Li, B. & Dewey, C.N. RSEM: accurate transcript quantification from RNA-Seq data with or without a reference genome. *BMC Bioinformatics* **12**, 323 (2011).

71. Efron, B. & Morris, C. Steins Estimation Rule and Its Competitors - Empirical Bayes Approach. *Journal of the American Statistical Association* **68**, 117-130 (1973).

72. Morris, C.N. Parametric Empirical Bayes Inference - Theory and Applications - Rejoinder. *Journal of the American Statistical Association* **78**, 63-65 (1983).

73. Kirby, R. Optimising the management of early prostate cancer. *Practitioner* **258**, 15-8, 2 (2014).

74. Sountoulides, P. & Moutzouris, G. Prostate-specific antigen screening, why have the guidelines changed? *Expert Rev Anticancer Ther* **14**, 1277-81 (2014).

75. Sharon, E. et al. Serum mesothelin and megakaryocyte potentiating factor in pancreatic and biliary cancers. *Clin Chem Lab Med* **50**, 721-5 (2012).

76. Rowley, J.D. Letter: A new consistent chromosomal abnormality in chronic myelogenous leukaemia identified by quinacrine fluorescence and Giemsa staining. *Nature* **243**, 290-3 (1973).

77. Soverini, S., Martinelli, G., Iacobucci, I. & Baccarani, M. Imatinib mesylate for the treatment of chronic myeloid leukemia. *Expert Rev Anticancer Ther* **8**, 853-64 (2008).

78.   Pan, Q., Shai, O., Lee, L.J., Frey, B.J. & Blencowe, B.J. Deep surveying of alternative splicing complexity in the human transcriptome by high-throughput sequencing. *Nat Genet* **40**, 1413-5 (2008).

79.   Carrigan, P.E., Bingham, J.L., Srinvasan, S., Brentnall, T.A. & Miller, L.J. Characterization of alternative spliceoforms and the RNA splicing machinery in pancreatic cancer. *Pancreas* **40**, 281-8 (2011).

80.   Waddell, N. et al. Whole genomes redefine the mutational landscape of pancreatic cancer. *Nature* **518**, 495-501 (2015).

81.   Klijn, C. et al. A comprehensive transcriptional portrait of human cancer cell lines. *Nat Biotechnol* **33**, 306-12 (2015).

82.   Kisseleva, T., Bhattacharya, S., Braunstein, J. & Schindler, C.W. Signaling through the JAK/STAT pathway, recent advances and future challenges. *Gene* **285**, 1-24 (2002).

83.   Zhong, Z., Wen, Z. & Darnell, J.E., Jr. Stat3: a STAT family member activated by tyrosine phosphorylation in response to epidermal growth factor and interleukin-6. *Science* **264**, 95-8 (1994).

84.   Zhang, Y. et al. Interleukin-6 is required for pancreatic cancer progression by promoting MAPK signaling activation and oxidative stress resistance. *Cancer Res* **73**, 6359-74 (2013).

85.   Wei, D. et al. Stat3 activation regulates the expression of vascular endothelial growth factor and human pancreatic cancer angiogenesis and metastasis. *Oncogene* **22**, 319-29 (2003).

86.   Toyonaga, T. et al. Blockade of constitutively activated Janus kinase/signal transducer and activator of transcription-3 pathway inhibits growth of human pancreatic cancer. *Cancer Lett* **201**, 107-16 (2003).

87.   Miyazaki, T. et al. Functional activation of Jak1 and Jak3 by selective association with IL-2 receptor subunits. *Science* **266**, 1045-7 (1994).

88.   Waickman, A.T., Park, J.Y. & Park, J.H. The common gamma-chain cytokine receptor: tricks-and-treats for T cells. *Cell Mol Life Sci* **73**, 253-69 (2016).

89.   Buckley, R.H. et al. Human severe combined immunodeficiency: genetic, phenotypic, and functional diversity in one hundred eight infants. *J Pediatr* **130**, 378-87 (1997).

90.   Levesque, M.C. et al. IL-4 and interferon gamma regulate expression of inducible nitric oxide synthase in chronic lymphocytic leukemia cells. *Leukemia* **17**, 442-50 (2003).

91.   Rich, B.E., Campos-Torres, J., Tepper, R.I., Moreadith, R.W. & Leder, P. Cutaneous lymphoproliferation and lymphomas in interleukin 7 transgenic mice. *J Exp Med* **177**, 305-16 (1993).

92.   Ullrich, K. et al. The IL-15 cytokine system provides growth and survival signals in Hodgkin lymphoma and enhances the inflammatory phenotype of HRS cells. *Leukemia* **29**, 1213-8 (2015).

93.   Todaro, M. et al. Colon cancer stem cells dictate tumor growth and resist cell death by production of interleukin-4. *Cell Stem Cell* **1**, 389-402 (2007).

94.   Todaro, M. et al. Autocrine production of interleukin-4 and interleukin-10 is required for survival and growth of thyroid cancer cells. *Cancer Res* **66**, 1491-9 (2006).

95.   Roca, H. et al. IL-4 induces proliferation in prostate cancer PC3 cells under nutrient-depletion stress through the activation of the JNK-pathway and survivin up-regulation. *J Cell Biochem* **113**, 1569-80 (2012).

96.   Walter, K. et al. Overexpression of smoothened activates the sonic hedgehog signaling pathway in pancreatic cancer-associated fibroblasts. *Clin Cancer Res* **16**, 1781-9 (2010).

97.	Shen, B. et al. Efficient genome modification by CRISPR-Cas9 nickase with minimal off-target effects. *Nat Methods* **11**, 399-402 (2014).
98.	Takehara, A. et al. Novel tumor marker REG4 detected in serum of patients with resectable pancreatic cancer and feasibility for antibody therapy targeting REG4. *Cancer Sci* **97**, 1191-7 (2006).
99.	Kayed, H. et al. FXYD3 is overexpressed in pancreatic ductal adenocarcinoma and influences pancreatic cancer cell growth. *Int J Cancer* **118**, 43-54 (2006).
100.	Huang, T. et al. Expression and diagnostic value of HE4 in pancreatic adenocarcinoma. *Int J Mol Sci* **16**, 2956-70 (2015).
101.	Sato, N. et al. Epigenetic inactivation of TFPI-2 as a common mechanism associated with growth and invasion of pancreatic ductal adenocarcinoma. *Oncogene* **24**, 850-8. (2005).
102.	Hong, S.M. et al. Multiple genes are hypermethylated in intraductal papillary mucinous neoplasms of the pancreas. *Mod Pathol* **21**, 1499-507 (2008).
103.	Sun, Y., Yang, S., Sun, N. & Chen, J. Differential expression of STAT1 and p21 proteins predicts pancreatic cancer progression and prognosis. *Pancreas* **43**, 619-23 (2014).
104.	Tanaka, M. et al. EVI1 oncogene promotes KRAS pathway through suppression of microRNA-96 in pancreatic carcinogenesis. *Oncogene* **33**, 2454-63 (2014).
105.	Bonder, C.S., Dickensheets, H.L., Finlay-Jones, J.J., Donnelly, R.P. & Hart, P.H. Involvement of the IL-2 receptor gamma-chain (gammac) in the control by IL-4 of human monocyte and macrophage proinflammatory mediator production. *J Immunol* **160**, 4048-56 (1998).
106.	Hemar, A. et al. Endocytosis of interleukin 2 receptors in human T lymphocytes: distinct intracellular localization and fate of the receptor alpha, beta, and gamma chains. *J Cell Biol* **129**, 55-64 (1995).
107.	Agarwal, A. et al. Functional RNAi screen targeting cytokine and growth factor receptors reveals oncorequisite role for interleukin-2 gamma receptor in JAK3-mutation-positive leukemia. *Oncogene* **34**, 2991-9 (2015).
108.	Boltz-Nitulescu, G. et al. Differentiation of rat bone marrow cells into macrophages under the influence of mouse L929 cell supernatant. *J Leukoc Biol* **41**, 83-91 (1987).
109.	Giron-Michel, J. et al. Detection of a functional hybrid receptor gammac/GM-CSFRbeta in human hematopoietic CD34+ cells. *J Exp Med* **197**, 763-75 (2003).
110.	Waghray, M. et al. GM-CSF Mediates Mesenchymal-Epithelial Crosstalk in Pancreatic Cancer. *Cancer Discov* (2016).
111.	Prokopchuk, O., Liu, Y., Henne-Bruns, D. & Kornmann, M. Interleukin-4 enhances proliferation of human pancreatic cancer cells: evidence for autocrine and paracrine actions. *Br J Cancer* **92**, 921-8 (2005).
112.	Kontermann, R.E. Dual targeting strategies with bispecific antibodies. *MAbs* **4**, 182-97 (2012).
113.	Debinski, W., Puri, R.K., Kreitman, R.J. & Pastan, I. A wide range of human cancers express interleukin 4 (IL4) receptors that can be targeted with chimeric toxin composed of IL4 and Pseudomonas exotoxin. *J Biol Chem* **268**, 14065-70 (1993).
114.	Ross, J.A. et al. Inhibition of JAK3 with a novel, selective and orally active small molecule induces therapeutic response in T-cell malignancies. *Leukemia* **28**, 941-4 (2014).
115.	Huang, C. et al. Inhibition of STAT3 activity with AG490 decreases the invasion of human pancreatic cancer cells in vitro. *Cancer Sci* **97**, 1417-23 (2006).
116.	Macha, M.A. et al. Guggulsterone decreases proliferation and metastatic behavior of pancreatic cancer cells by modulating JAK/STAT and Src/FAK signaling. *Cancer Lett* **341**, 166-77 (2013).

117. BusinessWire. Incyte Announces Decision to Discontinue JANUS Studies of Ruxolitinib plus Capecitabine in Patients with Advanced or Metastatic Pancreatic Cancer. (2016).
118. von Bernstorff, W. et al. Systemic and local immunosuppression in pancreatic cancer patients. *Clin Cancer Res* **7**, 925s-932s (2001).
119. Caprotti, R. et al. Free-from-progression period and overall short preoperative immunotherapy with IL-2 increases the survival of pancreatic cancer patients treated with macroscopically radical surgery. *Anticancer Res* **28**, 1951-4 (2008).
120. Uggeri, F. et al. Short-term preoperative IL-2 immunotherapy in operable pancreatic cancer: a randomized study. *Hepatogastroenterology* **56**, 861-5 (2009).
121. Nath, S. et al. MUC1 induces drug resistance in pancreatic cancer cells via upregulation of multidrug resistance genes. *Oncogenesis* **2**, e51 (2013).
122. Chaika, N.V. et al. MUC1 mucin stabilizes and activates hypoxia-inducible factor 1 alpha to regulate metabolism in pancreatic cancer. *Proc Natl Acad Sci U S A* **109**, 13787-92 (2012).
123. Zheng, L. & Jaffee, E.M. Annexin A2 is a new antigenic target for pancreatic cancer immunotherapy. *Oncoimmunology* **1**, 112-114 (2012).
124. Cao, R. et al. Elevated expression of myosin X in tumours contributes to breast cancer aggressiveness and metastasis. *Br J Cancer* **111**, 539-50 (2014).
125. Arjonen, A. et al. Mutant p53-associated myosin-X upregulation promotes breast cancer invasion and metastasis. *J Clin Invest* **124**, 1069-82 (2014).
126. Ju, X.D. et al. Both Myosin-10 isoforms are required for radial neuronal migration in the developing cerebral cortex. *Cereb Cortex* **24**, 1259-68 (2014).
127. Shatseva, T., Lee, D.Y., Deng, Z. & Yang, B.B. MicroRNA miR-199a-3p regulates cell proliferation and survival by targeting caveolin-2. *J Cell Sci* **124**, 2826-36 (2011).
128. Wang, L. et al. Hint1 inhibits growth and activator protein-1 activity in human colon cancer cells. *Cancer Res* **67**, 4700-8 (2007).
129. Weiske, J. & Huber, O. The histidine triad protein Hint1 triggers apoptosis independent of its enzymatic activity. *J Biol Chem* **281**, 27356-66 (2006).
130. de Graauw, M. et al. Annexin A2 depletion delays EGFR endocytic trafficking via cofilin activation and enhances EGFR signaling and metastasis formation. *Oncogene* **33**, 2610-9 (2014).
131. Kaur, S., Kumar, S., Momi, N., Sasson, A.R. & Batra, S.K. Mucins in pancreatic cancer and its microenvironment. *Nat Rev Gastroenterol Hepatol* **10**, 607-20 (2013).
132. Besmer, D.M. et al. Pancreatic ductal adenocarcinoma mice lacking mucin 1 have a profound defect in tumor growth and metastasis. *Cancer Res* **71**, 4432-42 (2011).
133. Bakkenist, C.J. & Kastan, M.B. DNA damage activates ATM through intermolecular autophosphorylation and dimer dissociation. *Nature* **421**, 499-506 (2003).
134. Shiloh, Y. & Ziv, Y. The ATM protein kinase: regulating the cellular response to genotoxic stress, and more. *Nat Rev Mol Cell Biol* **14**, 197-210 (2013).
135. Perlman, S.L., Boder Deceased, E., Sedgewick, R.P. & Gatti, R.A. Ataxia-telangiectasia. *Handb Clin Neurol* **103**, 307-32 (2012).
136. FitzGerald, M.G. et al. Heterozygous ATM mutations do not contribute to early onset of breast cancer. *Nat Genet* **15**, 307-10 (1997).
137. Biankin, A.V. et al. Pancreatic cancer genomes reveal aberrations in axon guidance pathway genes. *Nature* **491**, 399-405 (2012).
138. Kim, H. et al. Having pancreatic cancer with tumoral loss of ATM and normal TP53 protein expression is associated with a poorer prognosis. *Clin Cancer Res* **20**, 1865-72 (2014).

139. Russell, R. et al. Loss of ATM accelerates pancreatic cancer formation and epithelial-mesenchymal transition. *Nat Commun* **6**, 7677 (2015).

140. Jiang, H. et al. The combined status of ATM and p53 link tumor development with therapeutic response. *Genes Dev* **23**, 1895-909 (2009).

141. Kwok, M. et al. ATR inhibition induces synthetic lethality and overcomes chemoresistance in TP53- or ATM-defective chronic lymphocytic leukemia cells. *Blood* **127**, 582-95 (2016).

142. Tribius, S., Pidel, A. & Casper, D. ATM protein expression correlates with radioresistance in primary glioblastoma cells in culture. *Int J Radiat Oncol Biol Phys* **50**, 511-23 (2001).

143. Austen, B. et al. Mutation status of the residual ATM allele is an important determinant of the cellular response to chemotherapy and survival in patients with chronic lymphocytic leukemia containing an 11q deletion. *J Clin Oncol* **25**, 5448-57 (2007).

144. Palmieri, D. et al. HMGA proteins promote ATM expression and enhance cancer cell resistance to genotoxic agents. *Oncogene* **30**, 3024-35 (2011).

145. Reinhardt, H.C., Aslanian, A.S., Lees, J.A. & Yaffe, M.B. p53-deficient cells rely on ATM- and ATR-mediated checkpoint signaling through the p38MAPK/MK2 pathway for survival after DNA damage. *Cancer Cell* **11**, 175-89 (2007).

146. Song, H., Hollstein, M. & Xu, Y. p53 gain-of-function cancer mutants induce genetic instability by inactivating ATM. *Nat Cell Biol* **9**, 573-80 (2007).

147. Thompson, L.H. Recognition, signaling, and repair of DNA double-strand breaks produced by ionizing radiation in mammalian cells: the molecular choreography. *Mutat Res* **751**, 158-246 (2012).

148. Lee, J.H. & Paull, T.T. ATM activation by DNA double-strand breaks through the Mre11-Rad50-Nbs1 complex. *Science* **308**, 551-4 (2005).

149. Jazayeri, A., Balestrini, A., Garner, E., Haber, J.E. & Costanzo, V. Mre11-Rad50-Nbs1-dependent processing of DNA breaks generates oligonucleotides that stimulate ATM activity. *EMBO J* **27**, 1953-62 (2008).

150. Soutoglou, E. & Misteli, T. Activation of the cellular DNA damage response in the absence of DNA lesions. *Science* **320**, 1507-10 (2008).

151. Sun, Y., Xu, Y., Roy, K. & Price, B.D. DNA damage-induced acetylation of lysine 3016 of ATM activates ATM kinase activity. *Mol Cell Biol* **27**, 8502-9 (2007).

152. Kozlov, S.V. et al. Autophosphorylation and ATM activation: additional sites add to the complexity. *J Biol Chem* **286**, 9107-19 (2011).

153. Stein, P.S. & Daniels-McQueen, S. Modular organization of turtle spinal interneurons during normal and deletion fictive rostral scratching. *J Neurosci* **22**, 6800-9 (2002).

154. Difilippantonio, S. & Nussenzweig, A. The NBS1-ATM connection revisited. *Cell Cycle* **6**, 2366-70 (2007).

155. Stracker, T.H. & Petrini, J.H. The MRE11 complex: starting from the ends. *Nat Rev Mol Cell Biol* **12**, 90-103 (2011).

156. Lim, D.S. et al. ATM phosphorylates p95/nbs1 in an S-phase checkpoint pathway. *Nature* **404**, 613-7 (2000).

157. Gatei, M. et al. ATM protein-dependent phosphorylation of Rad50 protein regulates DNA repair and cell cycle control. *J Biol Chem* **286**, 31542-56 (2011).

158. Huang, X., Halicka, H.D. & Darzynkiewicz, Z. Detection of histone H2AX phosphorylation on Ser-139 as an indicator of DNA damage (DNA double-strand breaks). *Curr Protoc Cytom* **Chapter 7**, Unit 7 27 (2004).

159. Chao, C. et al. Cell type- and promoter-specific roles of Ser18 phosphorylation in regulating p53 responses. *J Biol Chem* **278**, 41028-33 (2003).

160. Chao, C., Saito, S., Anderson, C.W., Appella, E. & Xu, Y. Phosphorylation of murine p53 at ser-18 regulates the p53 responses to DNA damage. *Proc Natl Acad Sci U S A* **97**, 11936-41 (2000).

161. Mirzayans, R., Andrais, B., Scott, A. & Murray, D. New insights into p53 signaling and cancer cell response to DNA damage: implications for cancer therapy. *J Biomed Biotechnol* **2012**, 170325 (2012).

162. Choi, M., Shi, J., Jung, S.H., Chen, X. & Cho, K.H. Attractor landscape analysis reveals feedback loops in the p53 network that control the cellular response to DNA damage. *Sci Signal* **5**, ra83 (2012).

163. el-Deiry, W.S. et al. WAF1, a potential mediator of p53 tumor suppression. *Cell* **75**, 817-25 (1993).

164. Sancar, A., Lindsey-Boltz, L.A., Unsal-Kacmaz, K. & Linn, S. Molecular mechanisms of mammalian DNA repair and the DNA damage checkpoints. *Annu Rev Biochem* **73**, 39-85 (2004).

165. Zhao, H., Watkins, J.L. & Piwnica-Worms, H. Disruption of the checkpoint kinase 1/cell division cycle 25A pathway abrogates ionizing radiation-induced S and G2 checkpoints. *Proc Natl Acad Sci U S A* **99**, 14795-800 (2002).

166. Matsuoka, S. et al. ATM and ATR substrate analysis reveals extensive protein networks responsive to DNA damage. *Science* **316**, 1160-6 (2007).

167. Jung, M. et al. Human fibroblasts for large-scale "omics" investigations of ATM gene function. *Adv Exp Med Biol* **720**, 181-90 (2011).

168. Choi, S. et al. Quantitative proteomics reveal ATM kinase-dependent exchange in DNA damage response complexes. *J Proteome Res* **11**, 4983-91 (2012).

169. Brown, E.J. & Baltimore, D. Essential and dispensable roles of ATR in cell cycle arrest and genome maintenance. *Genes Dev* **17**, 615-28 (2003).

170. Zou, L. & Elledge, S.J. Sensing DNA damage through ATRIP recognition of RPA-ssDNA complexes. *Science* **300**, 1542-8 (2003).

171. Li, Z., Pearlman, A.H. & Hsieh, P. DNA mismatch repair and the DNA damage response. *DNA Repair (Amst)* **38**, 94-101 (2016).

172. Jette, N. & Lees-Miller, S.P. The DNA-dependent protein kinase: A multifunctional protein kinase with roles in DNA double strand break repair and mitosis. *Prog Biophys Mol Biol* **117**, 194-205 (2015).

173. Riballo, E. et al. A pathway of double-strand break rejoining dependent upon ATM, Artemis, and proteins locating to gamma-H2AX foci. *Mol Cell* **16**, 715-24 (2004).

174. Goodarzi, A.A. et al. ATM signaling facilitates repair of DNA double-strand breaks associated with heterochromatin. *Mol Cell* **31**, 167-77 (2008).

175. Muraki, K., Han, L., Miller, D. & Murnane, J.P. The role of ATM in the deficiency in nonhomologous end-joining near telomeres in a human cancer cell line. *PLoS Genet* **9**, e1003386 (2013).

176. Moyal, L. et al. Requirement of ATM-dependent monoubiquitylation of histone H2B for timely repair of DNA double-strand breaks. *Mol Cell* **41**, 529-42 (2011).

177. Murr, R. et al. Histone acetylation by Trrap-Tip60 modulates loading of repair proteins and repair of DNA double-strand breaks. *Nat Cell Biol* **8**, 91-9 (2006).

178. Cui, Y. et al. Genetically defined subsets of human pancreatic cancer show unique in vitro chemosensitivity. *Clin Cancer Res* **18**, 6519-30 (2012).

179. Radford, I.R. & Murphy, T.K. Radiation response of mouse lymphoid and myeloid cell lines. Part III. Different signals can lead to apoptosis and may influence sensitivity to killing by DNA double-strand breakage. *Int J Radiat Biol* **65**, 229-39 (1994).

180. Gregoire, V. et al. The role of fludarabine-induced apoptosis and cell cycle synchronization in enhanced murine tumor radiation response in vivo. *Cancer Res* **54**, 6201-9 (1994).

181. Gleeson, F.C. et al. Targeted next generation sequencing of endoscopic ultrasound acquired cytology from ampullary and pancreatic adenocarcinoma has the potential to aid patient stratification for optimal therapy selection. *Oncotarget* (2016).

182. Lord, C.J., McDonald, S., Swift, S., Turner, N.C. & Ashworth, A. A high-throughput RNA interference screen for DNA repair determinants of PARP inhibitor sensitivity. *DNA Repair (Amst).* **7**, 2010-9. Epub 2008 Oct 15. (2008).

183. Gilardini Montani, M.S. et al. ATM-depletion in breast cancer cells confers sensitivity to PARP inhibition. *J Exp Clin Cancer Res* **32**, 95 (2013).

184. Mateo, J. et al. DNA-Repair Defects and Olaparib in Metastatic Prostate Cancer. *N Engl J Med* **373**, 1697-708 (2015).

Michael Ayars | 847-204-8673 | mayars1@jhmi.edu

EDUCATION

THE JOHNS HOPKINS UNIVERSITY SCHOOL OF MEDICINE   **Aug 2010-September 2016 (expected)**
- Ph.D. Candidate Dept. of Pathobiology, *RNA expression patterns in pancreatic intraepithelial neoplasia*

THE JOHNS HOPKINS BLOOMBERG SCHOOL OF PUBLIC HEALTH   **2008-2010**
- Master of Science Dept. of Molecular Microbiology and Immunology,

ROCHESTER INSTITUTE OF TECHNOLOGY   **2004-2008**
- Bachelor of Science in Biotechnology and Bioinformatics,   November 2015

RESEARCH

Graduate Research Assistant, The Johns Hopkins University School of Medicine   **Aug 2010-Present**
Graduate Research Assistant, Johns Hopkins Bloomberg School of Public Health   **2009-2010**

PUBLICATIONS

- Ayars, M., O'Sullivan, E., MacGregor, A., Shindo, K., Goggins, M. RNA expression patterns in pancreatic intraepithelial neoplasia. Manuscript in preparation.
- Ayars, M., Goggins, M. Pancreatic cancer: Classifying pancreatic cancer using gene expression profiling. *Nature Rev Gastroenterol Hepatol* advance online publication (2015).
- Ayars, M., Goggins, M. in *Molecular Alterations of Pancreatic Cancer* (eds Simeone, D. & Maitra, A.) 185–208 (Springer, 2013).
- Omura N, Mizuma M, Macgregor A, Hong SM, Ayars M, Almario JA, Borges M, Kanda M, Li A, Vincent A, Maitra A, Goggins M. Overexpression of ankyrin1 promotes pancreatic cancer cell growth. Oncotarget. 2016;
- Vincent A, Hong SM, Hu C, Omura N, Young A, Kim H, Yu J, Knight S, Ayars M, Griffith M, Van Seuningen I, Maitra A, Goggins M. Epigenetic silencing of EYA2 in pancreatic adenocarcinomas promotes tumor growth. Oncotarget. 2014;5(9):2575-87.
- Karafin M, Jallo GI, Ayars M, Eberhart CG, Rodriguez FJ. Rosette forming glioneuronal tumor in association with Noonan syndrome: pathobiological implications. Clin Neuropathol. 2011;30(6):297-300.